GeNIe: Generative Hard Negative Images Through Diffusion

Anonymous authors
Paper under double-blind review

Abstract

Data augmentation is crucial in training deep models, preventing them from overfitting to limited data. Recent advances in generative AI, e.g., diffusion models, have enabled more sophisticated augmentation techniques that produce data resembling natural images. We introduce `GeNIe` a novel augmentation method which leverages a latent diffusion model conditioned on a text prompt to combine two contrasting data points (an image from the source category and a text prompt from the target category) to generate challenging augmentations. To achieve this, we adjust the noise level (equivalently, number of diffusion iterations) to ensure the generated image retains low-level and background features from the source image while representing the target category, resulting in a *hard negative* sample for the source category. We further automate and enhance `GeNIe` by adaptively adjusting the noise level selection on a per image basis (coined as `GeNIe-Ada`), leading to further performance improvements. Our extensive experiments, in both few-shot and long-tail distribution settings, demonstrate the effectiveness of our novel augmentation method and its superior performance over the prior art. Our code is available at: https://anonymous.4open.science/r/GeNIe-F6C6

1 Introduction

Augmentation has become an integral part of training deep learning models, particularly when faced with limited training data. For instance, when it comes to image classification with limited number of samples per class, model generalization ability can be significantly hindered. Simple transformations like rotation, cropping, and adjustments in brightness artificially diversify the training set, offering the model a more comprehensive grasp of potential data variations. Hence, augmentation can serve as a practical strategy to boost the model's learning capacity, minimizing the risk of overfitting and facilitating effective knowledge transfer from limited labelled data to real-world scenarios. Various image augmentation methods, encompassing standard transformations, and learning-based approaches have been proposed (Cubuk et al., 2019b;a; Yun et al., 2019b; Zhang et al., 2018; Trabucco et al., 2024). Some augmentation strategies combine two images possibly from two different categories to generate a new sample image. The simplest ones in this category are MixUp (Zhang et al., 2018) and CutMix (Yun et al., 2019a) where two images are combined in the pixel space. However, the resulting augmentations often do not lie within the manifold of natural images and act as out-of-distribution samples that will not be encountered during testing.

Recently, leveraging generative models for data augmentation has gained an upsurge of attention (Trabucco et al., 2024; Roy et al., 2023; Luzi et al., 2022; He et al., 2022b). These interesting studies, either based on fine-tuning or prompt engineering of diffusion models, are mostly focused on generating *generic augmentations* without considering the impact of other classes and incorporating that information into the generative process for a classification context. We take a different approach to generate challenging augmentations near the decision boundaries of a downstream classifier. Inspired by diffusion-based image editing methods (Meng et al., 2021; Luzi et al., 2022) some of which are previously used for data augmentation, we propose to use conditional latent diffusion models (Rombach et al., 2022) for generating *hard negative* images. Our core idea (coined as `GeNIe`) is to sample source images from various categories and prompt the diffusion model with a contradictory text corresponding to a different target category. We demonstrate that the choice of noise level (or equivalently number of iterations) for the diffusion process plays a pivotal role in generating images

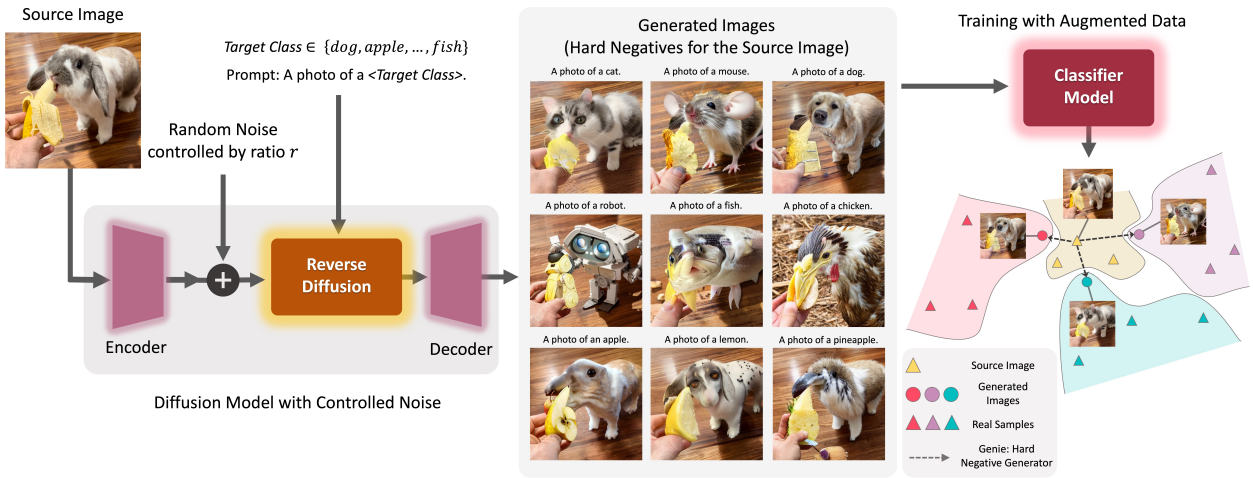

Figure 1: **Generative Hard Negative Images Through Diffusion (GeNIe):** generates hard negative images that belong to the target category but are similar to the source image from low-level feature and contextual perspectives. GeNIe starts from a source image passing it through a partial noise addition process, and conditioning it on a different target category. By controlling the amount of noise, the reverse latent diffusion process generates images that serve as *hard negatives* for the source category.

that semantically belong to the target category while retaining low-level features from the source image. We argue that these generated samples serve as *hard negatives* (Xuan et al., 2021; Mao et al., 2017) for the source category (or from a dual perspective hard positives for the target category). To further enhance GeNIe, we propose an adaptive noise level selection strategy (dubbed as GeNIe-Ada) enabling it to adjust noise levels automatically per sample.

To establish the impact of GeNIe, we focus on two challenging scenarios: *long-tail* and *few-shot* settings. In real-world applications, data often follows a long-tail distribution, where common scenarios dominate and rare occurrences are underrepresented. For instance, a person jaywalking a highway causes models to struggle with such unusual scenarios. Combating such a bias or lack of sufficient data samples during model training is essential in building robust models for self-driving cars or surveillance systems, to name a few. Same challenge arises in few-shot learning settings where the model has to learn from only a handful of samples. Our extensive quantitative and qualitative experimentation, on a suite of few-shot and long-tail distribution settings, corroborate the effectiveness of the proposed novel augmentation method (GeNIe, GeNIe-Ada) in generating hard negatives, corroborating its significant impact on categories with a limited number of samples. A high-level sketch of GeNIe is illustrated in Fig. 1. Our main contributions are summarized below:

- We introduce GeNIe, a novel yet elegantly simple diffusion-based augmentation method to create challenging augmentations in the manifold of natural images. For the first time, to our best knowledge, GeNIe achieves this by combining two sources of information (a source image, and a contradictory target prompt) through a noise-level adjustment mechanism.

- We further extend GeNIe by automating the noise-level adjustment strategy on a per-sample basis (called GeNIe-Ada), to enable generating hard negative samples in the context of image classification, leading also to further performance enhancement.

- To substantiate the impact of GeNIe, we present a suite of quantitative and qualitative results including extensive experimentation on two challenging tasks: few-shot and long tail distribution settings corroborating that GeNIe (and its extension GeNIe-Ada) significantly improve the downstream classification performance.

2 Related Work

Data Augmentations. Simple flipping, cropping, colour jittering, and blurring are some forms of image augmentations (Shorten & Khoshgoftaar, 2019). These augmentations are commonly adopted in training

deep learning models. However, using these data augmentations is not trivial in some domains. For example, using blurring might remove important low-level information from medical images. More advanced approaches, such as MixUp (Zhang et al., 2018) and CutMix (Yun et al., 2019a), mix images and their labels accordingly (Hendrycks et al., 2020; Liu et al., 2022; Kim et al., 2020; Cubuk et al., 2020). However, the resulting augmentations are not natural images anymore, and thus, act as out-of-distribution samples that will not be seen at test time. Another strand of research tailors the augmentation strategy through a learning process to fit the training data (Ding et al., 2024; Cubuk et al., 2019b;a). Unlike the above methods, we propose to utilize pre-trained latent diffusion models to generate hard negatives (in contrast to generic augmentations) through a noise adaptation strategy discussed in Section 3.

Data Augmentation with Generative Models. Using synthesized images from generative models to augment training data has been studied before in many domains (Frid-Adar et al., 2018; Sankaranarayanan et al., 2018), including domain adaptation (Huang et al., 2018), visual alignment (Peebles et al., 2022), and mitigation of dataset bias (Sharmanska et al., 2020; Hemmat et al., 2023; Prabhu et al., 2024). For example, (Prabhu et al., 2024) introduces a methodology aimed at enhancing test set evaluation through augmentation. While previous methods predominantly relied on GANs (Zhang et al., 2021c; Li et al., 2022b; Tritrong et al., 2021) as the generative model, more recent studies promote using diffusion models to augment the data (Rombach et al., 2022; He et al., 2022b; Shipard et al., 2023; Trabucco et al., 2024; Azizi et al., 2023; Luo et al., 2023; Roy et al., 2023; Jain et al., 2022; Feng et al., 2023; Dunlap et al., 2023b; Chegini & Feizi, 2023). More specifically, (Trabucco et al., 2024; Roy et al., 2023; He et al., 2022b; Azizi et al., 2023) study the effectiveness of text-to-image diffusion models in data augmentation by diversification of each class with synthetic images. (Roy et al., 2023) also utilizes a text-to-image diffusion model, but with a BLIP (Li et al., 2022d) model to generate meaningful captions from the existing images. (Jain et al., 2022) utilizes diffusion models for augmentation to correct model mistakes. (Feng et al., 2023) uses CLIP (Radford et al., 2021) to filter generated images. Generative models for data augmentation may produce out-of-distribution samples if the downstream task's data distribution differs. Fine-tuning on a small downstream dataset can address this. For example, DAFusion (Trabucco et al., 2024) fine-tunes a diffusion model using textual inversion (Gal et al., 2022a), while SiSTA (Thopalli et al., 2023) adapts a GAN for the task. (Graikos et al., 2023a) propose adapting generative models to downstream tasks by leveraging the internal representations of the denoiser network. Investigations by (Tian et al., 2023) explore the use of text-to-image synthetic images for generating positive samples in contrastive learning. (Dunlap et al., 2023b) utilizes text-based diffusion and a large language model (LLM) to diversify the training data. (Chegini & Feizi, 2023) uses an LLM to generate text descriptions of failure modes associated with spurious correlations, which are then used to generate synthetic data through generative models. The challenge here is that the LLM has little understanding of such failure scenarios and contexts.

We take a completely different approach here, without replying on any extra source of information (e.g., through an LLM). Inspired by image editing approaches such as Boomerang (Luzi et al., 2022) and SDEdit (Meng et al., 2021), we propose to adaptively guide a latent diffusion model to generate *hard negatives* images (Mao et al., 2017; Xuan et al., 2021) on a per-sample basis per category. In a nutshell, the aforementioned studies focus on improving the diversity of each class with effective prompts and diffusion models, however, we focus on generating effective *hard negative* samples for each class by combining two sources of contradicting information (images from the source category and text prompt from the target category).

Language Guided Recognition Models. Vision-Language foundation models (VLMs) (Alayrac et al., 2022; Radford et al., 2021; Rombach et al., 2022; Saharia et al., 2022; Ramesh et al., 2022; 2021) utilize human language to guide the generation of images or to extract features from images that are aligned with human language. CLIP (Radford et al., 2021) excels in zero-shot tasks by aligning images with text, while recent works improve prompts (Dunlap et al., 2023a; Petryk et al., 2022) or use diffusion models as classifiers (Li et al., 2023). Similarly, we leverage Stable Diffusion 1.5 (Rombach et al., 2022) to enhance downstream tasks by augmenting training data with hard negative samples based on category names.

Few-Shot Learning. In Few-shot Learning (FSL), we pre-train a model with abundant data to learn a rich representation, then fine-tune it on new tasks with only a few available samples. In supervised FSL (Chen et al., 2019a; Afrasiyabi et al., 2019; Qiao et al., 2018; Ye et al., 2020; Dvornik et al., 2019; Li et al., 2020; Sung et al., 2018; Zhou et al., 2021; Singh & Jamali-Rad, 2023), pretraining is done on a labeled dataset,

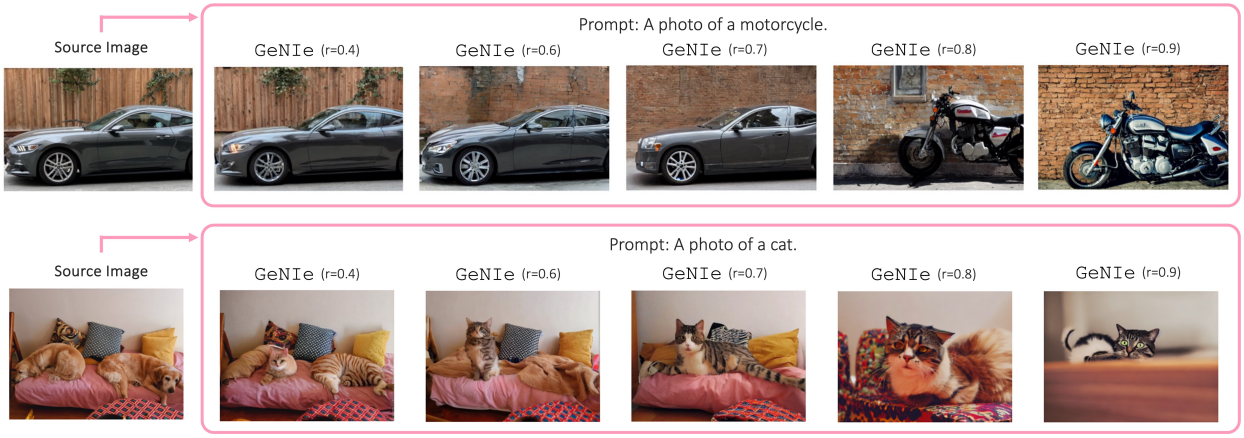

Figure 2: **Effect of noise ratio, r, in GeNIe:** we employ GeNIe to generate augmentations for the target classes (motorcycle and cat) with varying r. Smaller r yields images closely resembling the source semantics, creating an inconsistency with the intended target label. By tracing r from 0 to 1, augmentations gradually transition from source image characteristics to the target category. However, a distinct shift from the source to the target occurs at a specific r that may vary for different source images or target categories. For more examples, please refer to Fig. A9.

whereas in unsupervised FSL (Jang et al., 2022; Wang & Deng, 2022; Lu et al., 2022; Qin et al., 2020; Antoniou & Storkey, 2019; Khodadadeh et al., 2019; Hsu et al., 2018; Medina et al., 2020; Shirekar et al., 2023) the pretraining has to be conducted on an unlabeled dataset posing an extra challenge in the learning paradigm and neighboring these methods closer to the realm of self-supervised learning.

3 Proposed Method: GeNIe

Given a source image X_S from category S = <source category>, we are interested in generating a target image X_r from category T = <target category>. In doing so, we intend to ensure the low-level visual features or background context of the source image are preserved, so that we generate samples that would serve as *hard negatives* for the *source* image. To this aim, we adopt a conditional latent diffusion model (such as Stable Diffusion, (Rombach et al., 2022)) conditioned on a text prompt of the following format "A photo of a T = <target category>".

Key Idea. GeNIe in its basic form is a simple yet effective augmentation sample generator for improving a classifier $f_\theta(.)$ with the following two key aspects: (i) inspired by (Luzi et al., 2022; Meng et al., 2021) instead of adding the full amount of noise σ_{max} and going through all N_{max} (being typically 50) steps of denoising, we use less amount of noise ($r\sigma_{max}$, with $r \in (0, 1)$) and consequently fewer number of denoising iterations ($\lfloor rN_{max} \rfloor$); (ii) we prompt the diffusion model with a P mandating a target category T different than the source S. Hence, we denote the conditional diffusion process as $X_r = \texttt{STDiff}(X_S, P, r)$. In such a construct, the proximity of the final decoded image X_r to the source image X_S or the target category defined through the text prompt P depends on r. Hence, by controlling the amount of noise, we can generate images that blend characteristics of both the text prompt P and the source image X_S. If we do not provide much of visual details in the text prompt (e.g., desired background, etc.), we expect the decoded image X_r to follow the details of X_S while reflecting the semantics of the text prompt P. We argue, and demonstrate later, that the newly generated samples can serve as *hard negative* examples for the source category S since they share the low-level features of X_S while representing the semantics of the target category, T. Notably, the source category S can be randomly sampled or be carefully extracted from the confusion matrix of $f_\theta(.)$ based on real training data. The latter might result in even *harder negative* samples being now cognizant of model confusions. Finally, we will append our initial dataset with the newly generated hard negative samples through GeNIe and (re)train the classifier model.

Enhancing GeNIe: GeNIe-Ada. One of the remarkable aspects of GeNIe lies in its simple application, requiring only X_S, P, and r. However, selecting the appropriate value for r poses a challenge as it profoundly influences the outcome. When r is small, the resulting X_r tends to closely resemble X_S, and conversely, when

Algorithm 1: `GeNIe-Ada`

Require: X_S, X_T, $f_\theta(.)$, `STDiff`$(.)$, M
Extract $Z_S \leftarrow f_\theta(X_s)$, $Z_T \leftarrow f_\theta(X_T)$
for $m \in [1, M]$ **do**
  $r \leftarrow \frac{m}{M}$, $Z_r \leftarrow f_\theta(\texttt{STDiff}(X, P, r))$
  $d_m \leftarrow \frac{(Z_r - Z_S)^T (Z_T - Z_S)}{||Z_T - Z_S||_2}$
$m^* \leftarrow \text{argmax}_m |d_m - d_{m-1}|, \forall m \in [2, M]$
$r^* \leftarrow \frac{m^*}{n}$
Return: $X_{r^*} = \texttt{STDiff}(X_S, P, r^*)$

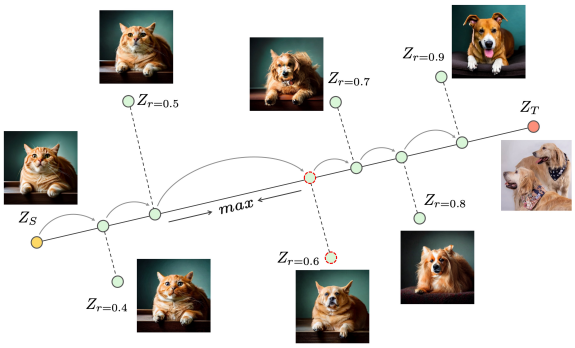

Figure 3: `GeNIe-Ada`: To choose r adaptively for each (source image, target category) pair, we propose tracing the semantic trajectory from Z_S (source image embeddings) to Z_T (target embeddings) through backbone feature extractor $f_\theta(\cdot)$ (Algorithm 1). We adaptively select the sample right after the largest semantic shift.

r is large (closer to 1), it tends to resemble the semantics of the target category. This phenomenon arises because a smaller noise level restricts the capacity of the diffusion model to deviate from the semantics of the input X_S. Thus, a critical question emerges: how can we select r for a particular source image to generate samples that preserve the low-level semantics of the source category S in X_S while effectively representing the semantics of the target category T? We propose a method to determine an ideal value for r.

Our intuition suggests that by varying the noise ratio r from 0 to 1, X_r will progressively resemble category S in the beginning and category T towards the end. However, somewhere between 0 and 1, X_r will undergo a rapid transition from category S to T. This phenomenon is empirically observed in our experiments with varying r, as depicted in Fig. 2. Although the exact reason for this rapid change remains uncertain, one possible explanation is that the intermediate points between two categories reside far from the natural image manifold, thus, challenging the diffusion model's capability to generate them. Ideally, we should select r corresponding to just after this rapid semantic transition, as at this point, X_r exhibits the highest similarity to the source image while belonging to the target category.

We propose to trace the semantic trajectory between X_S and X_T through backbone feature extractor $f_\theta(.)$. As shown in Algorithm 1, assuming access to the classifier backbone $f_\theta(.)$ and at least one example X_T from the target category, we convert both X_S and X_T into their respective latent vectors Z_S and Z_T by passing them through $f_\theta(.)$. Then, we sample M values for r uniformly distributed $\in (0, 1)$, generating their corresponding X_r and their latent vectors Z_r for all those r. Subsequently, we calculate $d_r = \frac{(Z_r - Z_S)^T (Z_T - Z_S)}{||Z_T - Z_S||_2}$ as the distance between Z_r and Z_S projected onto the vector connecting Z_S and Z_T. Our hypothesis posits that the rapid semantic transition corresponds to a sharp change in this projected distance. Therefore, we sample n values for r uniformly distributed between 0 and 1, and analyze the variations in d_r. We identify the largest gap in d_r and select the r value just after the gap when increasing r, as detailed in Algorithm 1 and illustrated in Fig. 3.

3.1 Psuedocode of GeNIe:

As illustrated in Algorithm 2, we provide a detailed pytorch-style pseudocode for `GeNIe`. First, a SDv1.5 pipeline initialized by loading all the components such as the VQ-VAE encoder and decoder, the CLIP text encoder and the DPM scheduler for the forward and reverse diffusion process. Then, the source image is input to the encoder to encode the image into latent space for the diffusion model. Next, the encoded image is partially noised based on the noise ratio r using the scheduler. The diffusion model then de-noises the partially noised latent embedding for a total of NUM INFERENCE STEPS $\times r$ steps, with an additional input of a text prompt from a contradictory target class. Finally, the decoder decodes the de-noised latent embedding into the generated hard-negative image, that contains the low-level features of the source image and the class/category of the contradictory text-prompt.

Algorithm 2: PyTorch-style Pseudocode of GeNIe.

```
# StableDiffusionPipeline: Pre-trained diffusion model
# DPMSolverMultistepScheduler: Scheduler for forward and reverse diffusion
# encode_latents: Encodes an image into latent space
# decode_latents: Decodes latents back into an image

def AugmentGeNIe(source_image, target_prompt, percent_noise):
    NUM_INFERENCE_STEPS = 50 # Number of steps for reverse diffusion
    NUM_TRAIN_STEPS = 1000 # Number of steps for forward diffusion

    # Initialize the stable diffusion pipeline and scheduler
    pipe = StableDiffusionPipeline.from_pretrained("stable-diffusion-v1-5")
    scheduler = DPMSolverMultistepScheduler.from_config(pipe.scheduler.config)

    # Encode the source image into latent space
    latents = encode_latents(source_image)

    # Forward Diffusion
    noise = torch.randn(latents.shape) # Generate random noise
    timestep = torch.Tensor([int(NUM_TRAIN_STEPS * percent_noise)]) # Calculate timestep
    latents_noise = scheduler.add_noise(latents, noise, timestep) # Add noise to latents

    # Reverse Diffusion
    latents = pipe(
        prompt=target_prompt,
        percent_noise=percent_noise,
        latents=latents_noise,
        num_inference_steps=NUM_INFERENCE_STEPS
    )

    # Decode latents back into an augmented image
    augmented_image = decode_latents(latents)

    return augmented_image
```

4 Experiments

Since the impact of augmentation is more pronounced when the training data is limited, we evaluate the impact of `GeNIe` on Few-Shot classification in Section 4.1, Long-Tailed classification in Section 4.3, and fine-grained classification in Section 4.2. For `GeNIe-Ada` in all scenarios, we utilize `GeNIe` to generate augmentations from the noise level set $\{0.5, 0.6, 0.7, 0.8, 0.9\}$. The selection of the appropriate noise level per source image and target is adaptive, achieved through Algorithm 1.

Baselines. We use Stable Diffusion 1.5 (Rombach et al., 2022) as our base diffusion model. In all settings, we use the same prompt format to generate images for the target class: i.e., "A photo of a <`target category`>", where we replace the `target category` with the target category label. We generate 512×512 images for all methods. For fairness, we generate the same number of new images for each class. We use a single NVIDIA RTX 3090 for image generation. We consider 4 diffusion-based baselines and a suite of traditional data augmentation baselines.

`Img2Img` (Luzi et al., 2022; Meng et al., 2021): We sample an image from a target class, add noise to its latent representation and then pass it along with a prompt for the target category through reverse diffusion. The focus here is on a target class for which we generate extra positive samples. Adding large amount of noise leads to generating an image less similar to the original image. We use two different noise magnitudes for this baseline: $r = 0.3$ and $r = 0.7$ and denote them by $\texttt{Img2Img}^L$ and $\texttt{Img2Img}^H$, respectively.

`Txt2Img` (Azizi et al., 2023; He et al., 2022b): For this baseline, we omit the forward diffusion process and only use the reverse process starting from a text prompt for the target class of interest. This is similar to the base text-to-image generation strategy adopted in (Rombach et al., 2022; He et al., 2022b; Shipard et al., 2023; Azizi et al., 2023; Luo et al., 2023). Fig. 4 illustrates a set of generated augmentation examples for `Txt2Img`, `Img2Img`, and `GeNIe`.

DAFusion (Trabucco et al., 2024): In this method, an embedding is optimized with a set of images for each class to correspond to the classes in the dataset. This approach is introduced in Textual Inversion (Gal et al., 2022c). We optimize an embedding for 5000 iterations for each class in the dataset, followed by augmentation similar as the DAFusion method.

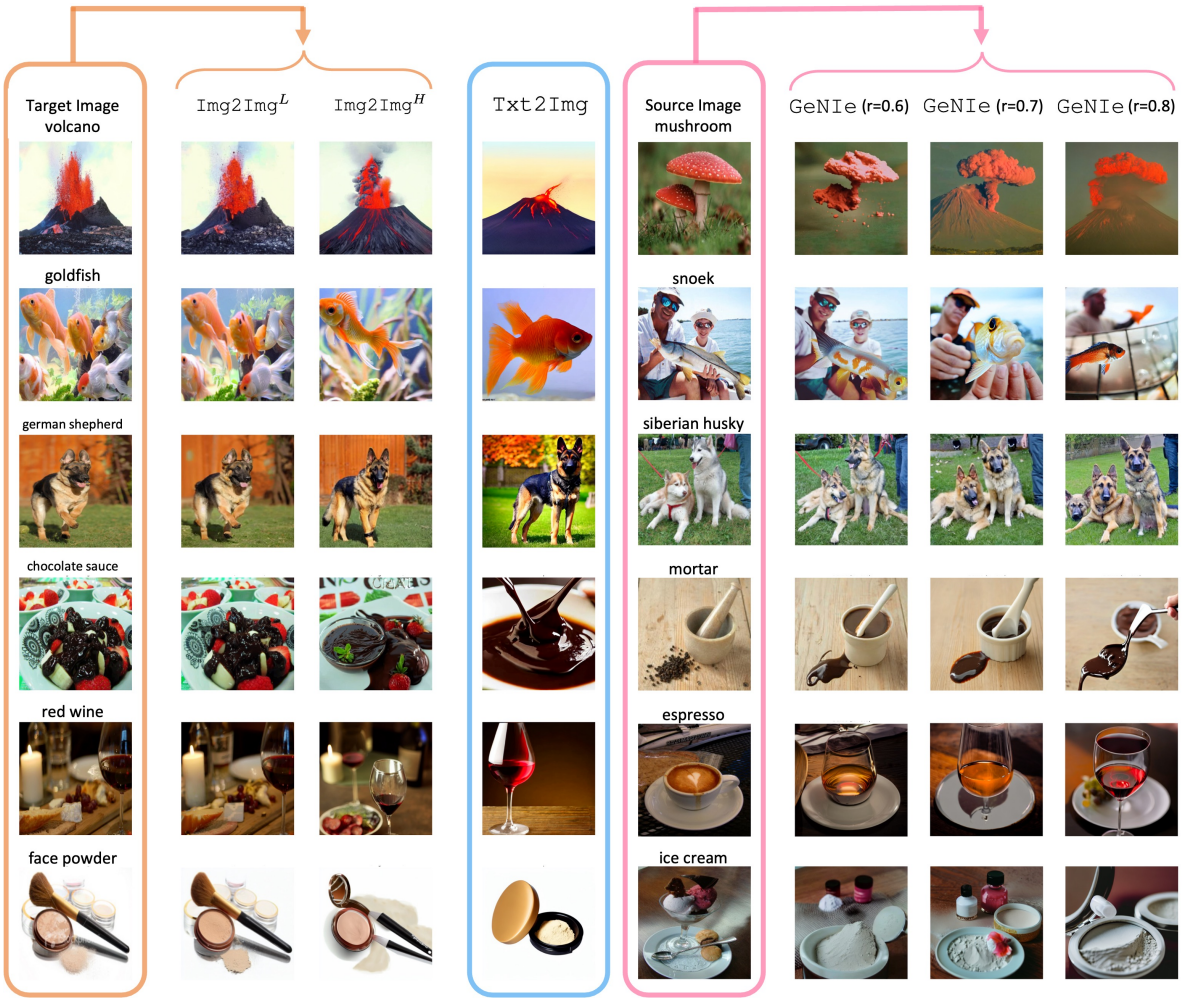

Figure 4: **Visualization of Generative Samples:** We compare `GeNIe` with two baselines: `Img2Img`^{L} **augmentation:** both image and text prompt are from the same category. Adding noise does not change the image much, so they are not hard examples. `Txt2Img` **augmentation:** We simply use the text prompt only to generate an image for the desired category (e.g., using a text2image method). Such images may be far from the domain of our task since the generation is not informed by any visual data from our task. `GeNIe` **augmentation:** We use the target category name in the text prompt only along with the source image.

Cap2Aug(Roy et al., 2023): It is a recent diffusion-based data augmentation strategy that uses image captions as text prompts for an image-to-image diffusion model.

Traditional Data Augmentation: We consider both weak and strong traditional augmentations. More specifically, for weak augmentation we use random resize crop with scaling $\in [0.2, 1.0]$ and horizontal flipping. For strong augmentation, we consider random color jitter, random grayscale, and Gaussian blur. For the sake of completeness, we also compare against data augmentations such as CutMix (Yun et al., 2019a) and MixUp (Zhang et al., 2018) that combine two images together.

4.1 Few-shot Classification

We assess the impact of `GeNIe` compared to other augmentations in a number of few-shot classification (FSL) scenarios, where the model has to learn only from the samples contained in the (N-way, K-shot) support set and infer on the query set. Note that this corresponds to an inference-only FSL setting where a pretraining stage on an abundant dataset is discarded. The goal is to assess how well the model can benefit from the augmentations while keeping the original $N \times K$ samples intact.

Table 1: ***mini*-ImageNet:** We use our augmentations on (5-way, 1-shot) and (5-way, 5-shot) few-shot settings of mini-Imagenet dataset with 3 different backbones (ResNet-18, 34, and 50). We compare with various baselines and show that our augmentations with UniSiam outperform all the baselines including `Txt2Img` and DAFusion augmentation. The number of generated images per class is 4 for 1-shot and 20 for 5-shot settings.

ResNet-18				
Augmentation	**Method**	**Pre-training**	**1-shot**	**5-shot**
-	iDeMe-Net 2019b	sup.	59.1±0.9	74.6±0.7
-	Robust + dist 2019	sup.	63.7±0.6	81.2±0.4
-	AFHN 2020	sup.	62.4±0.7	78.2±0.6
Weak	ProtoNet+SSL 2020	sup.+ssl	-	76.6
Weak	Neg-Cosine 2020	sup.	62.3±0.8	80.9±0.6
-	Centroid Align2019	sup.	59.9±0.7	80.4±0.7
-	Baseline 2019a	sup.	59.6±0.8	77.3±0.6
-	Baseline++ 2019a	sup.	59.0±0.8	76.7±0.6
Weak	PSST 2021	sup.+ssl	59.5±0.5	77.4±0.5
Weak	UMTRA 2019	unsup.	43.1±0.4	53.4±0.3
Weak	ProtoCLR 2020	unsup.	50.9±0.4	71.6±0.3
Weak	SimCLR 2020	unsup.	62.6±0.4	79.7±0.3
Weak	SimSiam 2021	unsup.	62.8±0.4	79.9±0.3
Weak	UniSiam+dist 2022	unsup.	**64.1±0.4**	**82.3±0.3**
Weak	UniSiam 2022	unsup.	63.1±0.8	81.4±0.5
Strong	UniSiam 2022	unsup.	62.8±0.8	81.2±0.6
CutMix 2019a	UniSiam 2022	unsup.	62.7±0.8	80.6±0.6
MixUp 2018	UniSiam 2022	unsup.	62.1±0.8	80.7±0.6
`Img2Img`^{L}2022	UniSiam 2022	unsup.	63.9±0.8	82.1±0.5
`Img2Img`^{H}2022	UniSiam 2022	unsup.	69.1±0.7	84.0±0.5
`Txt2Img`2023; 2022b	UniSiam 2022	unsup.	74.1±0.6	84.6±0.5
DAFusion 2024	UniSiam 2022	unsup.	64.3±1.8	82.0±1.4
`GeNIe` (Ours)	UniSiam 2022	unsup.	**75.5±0.6**	**85.4±0.4**
`GeNIe-Ada` (Ours)	UniSiam 2022	unsup.	**76.8±0.6**	**85.9±0.4**

ResNet-34				
Augmentation	**Method**	**Pre-training**	**1-shot**	**5-shot**
Weak	Baseline 2019a	sup.	49.8±0.7	73.5±0.7
Weak	Baseline++ 2019a	sup.	52.7±0.8	76.2±0.6
Weak	SimCLR 2020	unsup.	64.0±0.4	79.8±0.3
Weak	SimSiam 2021	unsup.	63.8±0.4	80.4±0.3
Weak	UniSiam+dist 2022	unsup.	**65.6±0.4**	**83.4±0.2**
Weak	UniSiam 2022	unsup.	64.3±0.8	82.3±0.5
Strong	UniSiam 2022	unsup.	64.5±0.8	82.1±0.6
CutMix 2019a	UniSiam 2022	unsup.	64.0±0.8	81.7±0.6
MixUp 2018	UniSiam 2022	unsup.	63.7±0.8	80.1±0.8
`Img2Img`^{L}2022	UniSiam 2022	unsup.	65.5±0.8	82.9±0.5
`Img2Img`^{H}2022	UniSiam 2022	unsup.	70.5±0.8	84.8±0.5
`Txt2Img`2023; 2022b	UniSiam 2022	unsup.	75.4±0.6	85.5±0.5
DAFusion 2024	UniSiam 2022	unsup.	64.7±1.9	83.2±1.4
`GeNIe` (Ours)	UniSiam 2022	unsup.	**77.1±0.6**	**86.3±0.4**
`GeNIe-Ada` (Ours)	UniSiam 2022	unsup.	**78.5±0.6**	**86.6±0.4**
ResNet-50				
Weak	PDA+Net 2021	unsup.	63.8±0.9	83.1±0.6
Weak	Meta-DM 2023	unsup.	66.7±0.4	85.3±0.2
Weak	UniSiam 2022	unsup.	64.6±0.8	83.4±0.5
Strong	UniSiam 2022	unsup.	64.8±0.8	83.2±0.5
CutMix 2019a	UniSiam 2022	unsup.	64.3±0.8	83.2±0.5
MixUp 2018	UniSiam 2022	unsup.	63.8±0.8	84.6±0.5
`Img2Img`^{L}2022	UniSiam 2022	unsup.	66.0±0.8	84.0±0.5
`Img2Img`^{H}2022	UniSiam 2022	unsup.	71.1±0.7	85.7±0.5
`Txt2Img`2023; 2022b	UniSiam 2022	unsup.	76.4±0.6	86.5±0.4
DAFusion 2024	UniSiam 2022	unsup.	65.7±1.8	83.9±1.2
`GeNIe` (Ours)	UniSiam 2022	unsup.	**77.3±0.6**	**87.2±0.4**
`GeNIe-Ada` (Ours)	UniSiam 2022	unsup.	**78.6±0.6**	**87.9±0.4**

Datasets. We conduct our few-shot experiments on two most commonly adopted few-shot classification datasets: *mini*-Imagenet (Ravi & Larochelle, 2017) and *tiered*-Imagenet (Ren et al., 2018). *mini*-Imagenet is a subset of ImageNet (Deng et al., 2009) for few-shot classification. It contains 100 classes with 600 samples each. We follow the predominantly adopted settings of (Ravi & Larochelle, 2017; Chen et al., 2019a) where we split the entire dataset into 64 classes for training, 16 for validation and 20 for testing. *tiered*-Imagenet is a larger subset of ImageNet with 608 classes and a total of $779,165$ images, which are grouped into 34 higher-level nodes in the *ImageNet* human-curated hierarchy. This set of nodes is partitioned into 20, 6, and 8 disjoint sets of training, validation, and testing nodes, and the corresponding classes form the respective meta-sets.

Evaluation. We evaluate the test-set accuracies of a state-of-the-art unsupervised few-shot learning method with `GeNIe` and compare them against the accuracies obtained using other augmentation methods. Specifically, we use UniSiam (Lu et al., 2022) pre-trained with ResNet-18, ResNet-34 and ResNet-50 backbones and follow its evaluation strategy of fine-tuning a logistic regressor to perform (N-way, K-shot) classification on the test sets of *mini*- and *tiered*-Imagenet. Following (Ravi & Larochelle, 2017), an episode consists of a labeled support-set and an unlabelled query-set. The support-set contains N randomly sampled classes where each class contains K samples, whereas the query-set contains Q randomly sampled unlabeled images per class. We conduct our experiments on the two most commonly adopted settings: (5-way, 1-shot) and (5-way, 5-shot) classification settings. Following the literature, we sample 16-shots per class for the query set in both settings. We report the test accuracies along with the 95% confidence interval over 600 and 1000 episodes for *mini*-ImageNet and *tiered*-ImageNet, respectively.

Implementation Details: `GeNIe` generates augmented images for each class using images from all other classes as the source image. We use $r = 0.8$ in our experiments. We generate 4 samples per class as augmentations in the 5-way, 1-shot setting and 20 samples per class as augmentations in the 5-way, 5-shot setting. For the sake of a fair comparison, we ensure that the total number of labelled samples in the support set after augmentation remains the same across all different traditional and generative augmentation methodologies. Due to the expensive training of embeddings for each class in each episode, we only evaluated the DA-Fusion baseline on the first 100 episodes.

Results: The results on *mini*-Imagenet and *tiered*-Imagenet for both (5-way, 1 and 5-shot) settings are summarized in Table 1 and Table 3, respectively. Regardless of the choice of backbone, we observe that

GeNIe helps consistently improve UniSiam's performance and outperform other supervised and unsupervised few-shot classification methods as well as other diffusion-based (Trabucco et al., 2024; Luzi et al., 2022; Rombach et al., 2021; He et al., 2022b) and classical (Yun et al., 2019a; Zhang et al., 2018) data augmentation techniques on both datasets, across both (5-way, 1 and 5-shot) settings. Our noise adaptive method of selecting optimal augmentations per source image (GeNIe-Ada) further improves GeNIe's performance across all three backbones, both few-shot settings, and both datasets (*mini* and *tiered*-Imagenet).

4.2 Fine-grained Few-shot Classification

To further investigate the impact of the proposed method, we compare GeNIe with other text-based data augmentation techniques across four distinct fine-grained datasets in a 20-way, 1-shot classification setting. We employ the pre-trained DINOV2 ViT-G (Oquab et al., 2023) backbone as a feature extractor to derive features from training images. Subsequently, an SVM classifier is trained on these features, and we report the Top-1 accuracy of the model on the test set.

Results: Table 2 summarizes the results. Additional details about this experiment can be found in Section A.7. GeNIe outperforms all other baselines, including Txt2Img, by margins upto 0.5% on CUB200, 6.6% on Cars196, 0.1% on Food101 and 5.3% on FGVC-Aircraft. GeNIe exhibits great effectiveness in more challenging datasets, outperforming the baseline with traditional augmentation by about 38% for the Cars dataset and by roughly 17% for the Aircraft dataset. It can be observed here that GeNIe-Ada performs on-par with GeNIe with a fixed noise level, eliminating the necessity for noise level search in GeNIe.

Table 2: **Few-shot Learning on Fine-grained dataset:** We utilize an SVM classifier trained atop the DINOV2 ViT-G pretrained backbone, reporting Top-1 accuracy for the test set of each dataset. The baseline is an SVM trained on the same backbone using weak augmentation.

Method	Birds CUB200 2011	Cars Cars196 2013	Foods Food101 2014	Aircraft Aircraft 2013
Baseline	90.3	49.8	82.9	29.2
Img2Img^{L}2022	90.7	50.4	87.4	31.0
Img2Img^{H}2022	91.3	56.4	91.7	34.7
Txt2Img2022b	92.0	81.3	93.0	41.7
GeNIe (r=0.5)	92.0	84.6	91.5	39.8
GeNIe (r=0.6)	92.2	87.1	92.5	45.0
GeNIe (r=0.7)	92.5	**87.9**	92.9	**47.0**
GeNIe (r=0.8)	92.5	87.7	**93.1**	46.5
GeNIe (r=0.9)	92.4	87.1	**93.1**	45.7
GeNIe-Ada	**92.6**	**87.9**	**93.1**	46.9

4.3 Long-Tailed Classification

We evaluate our method on long-tailed data, where the number of instances per class is unbalanced, with most categories having limited samples (tail). Our goal is to mitigate this bias by augmenting the tail of the distribution with generated samples. We evaluate GeNIe using two backbones: ViT with LViT (Xu et al., 2023) and ResNet50 with VL-LTR (Tian et al., 2022). Following LViT, we first train an MAE (He et al., 2021) and ViT on the unbalanced dataset without any augmentation. Next, we train the Balanced Fine-Tuning stage of LViT by incorporating the augmentation data generated using GeNIe or other baselines. For ResNet50, we use VL-LTR code to fine-tune the CLIP ResNet50 with generated augmentations by GeNIe.

Dataset: We perform experiments on ImageNet-LT (Liu et al., 2019). It contains 115.8K images from $1,000$ categories. The number of images per class varies from 1280 to 5. Imagenet-LT classes can be divided into 3 groups: "Few" with less than 20 images, "Med" with $20-100$ images, and "Many" with more than 100 images. Imagenet-LT uses the same validation set as ImageNet. We augment "Few" categories only and limit the number of generated images to 50 samples per class. For GeNIe, instead of randomly sampling the source images from other classes, we use a confusion matrix on the training data to find the top-4 most confused classes and only consider those classes for random sampling of the source image.

Results: Augmenting training data with GeNIe-Ada improves accuracy on the "Few" set by 11.7% and 4.4% compared with LViT only and LViT with Txt2Img augmentation baselines respectively. In ResNet50, GeNIe-Ada outperforms Cap2Aug baseline in "Few" categories by 7.6%. The results are summarized in Table 4. Please refer to Section A.9 for implementation details.

4.4 Ablation and Further Analysis

Semantic Shift from Source to Target Class. The core motivation behind GeNIe-Ada is that by varying the noise ratio r from 0 to 1, augmented sample X_r will progressively shift its semantic category from source

Table 3: ***tiered*-ImageNet:** Accuracies (% ± std) for 5-way, 1-shot and 5-way, 5-shot classification settings on the test-set. We compare against various SOTA supervised and unsupervised few-shot classification baselines as well as other augmentation methods, with UniSiam (Lu et al., 2022) pre-trained ResNet-18,50 backbones.

ResNet-18				
Augmentation	**Method**	**Pre-training**	**1-shot**	**5-shot**
Weak	SimCLR2020	unsup.	63.4±0.4	79.2±0.3
Weak	SimSiam 2021	unsup.	64.1±0.4	81.4±0.3
Weak	UniSiam 2022	unsup.	63.1±0.7	81.0±0.5
Strong	UniSiam 2022	unsup.	62.8±0.7	80.9±0.5
CutMix 2019a	UniSiam 2022	unsup.	62.1±0.7	78.9±0.6
MixUp 2018	UniSiam 2022	unsup.	62.1±0.7	78.4±0.6
`Img2Img`^{L}2022	UniSiam 2022	unsup.	63.9±0.7	81.8±0.5
`Img2Img`^{H}2022	UniSiam 2022	unsup.	68.7±0.7	83.5±0.5
`Txt2Img`2022b	UniSiam 2022	unsup.	72.9±0.6	84.2±0.5
DAFusion 2024	UniSiam 2022	unsup.	62.6±2.1	81.0±1.5
`GeNIe`(Ours)	UniSiam 2022	unsup.	**73.6±0.6**	**85.0±0.4**
`GeNIe-Ada`(Ours)	UniSiam 2022	unsup.	**75.1±0.6**	**85.5±0.5**
ResNet-50				
Weak	PDA+Net 2021	unsup.	69.0±0.9	84.2±0.7
Weak	Meta-DM 2023	unsup.	69.6±0.4	86.5±0.3
Weak	UniSiam + dist 2022	unsup.	69.6±0.4	86.5±0.3
Weak	UniSiam 2022	unsup.	66.8±0.7	84.7±0.5
Strong	UniSiam 2022	unsup.	66.5±0.7	84.5±0.5
CutMix 2019a	UniSiam 2022	unsup.	66.0±0.7	83.3±0.5
MixUp 2018	UniSiam 2022	unsup.	66.1±0.5	84.1±0.8
`Img2Img`^{L}2022	UniSiam 2022	unsup.	67.8±0.7	85.3±0.5
`Img2Img`^{H}2022	UniSiam 2022	unsup.	72.4±0.7	86.7±0.4
`Txt2Img`2022b	UniSiam 2022	unsup.	77.1±0.6	87.3±0.4
DAFusion 2024	UniSiam 2022	unsup.	66.5±2.2	84.8±1.4
`GeNIe` (Ours)	UniSiam 2022	unsup.	**78.0±0.6**	**88.0±0.4**
`GeNIe-Ada` (Ours)	UniSiam 2022	unsup.	**78.8±0.6**	**88.6±0.6**

Table 4: **Long-Tailed ImageNet-LT:** We compare different augmentation methods on ImageNet-LT and report Top-1 accuracy for "Few", "Medium", and "Many" sets. On the "Few" set and LiVT method, our augmentations improve the accuracy by 11.7 points compared to LiVT original augmentation and 4.4 points compared to `Txt2Img`. `GeNIe-Ada` outperforms Cap2Aug baseline in "Few" categories by 7.6%. Refer to Table A8 for a full comparison with prior Long-Tailed methods.

ResNet-50				
Method	Many	Med.	Few	Overall Acc
ResLT 2022	63.3	53.3	40.3	55.1
PaCo 2021b	68.2	58.7	41.0	60.0
LWS 2019	62.2	48.6	31.8	51.5
Zero-shot CLIP 2021	60.8	59.3	58.6	59.8
DRO-LT 2021	64.0	49.8	33.1	53.5
VL-LTR 2022	77.8	67.0	50.8	70.1
Cap2Aug 2023	78.5	**67.7**	51.9	70.9
`GeNIe-Ada`	**79.2**	64.6	**59.5**	**71.5**
ViT-B				
Method	Many	Med.	Few	Overall Acc
ViT 2021	50.5	23.5	6.9	31.6
MAE 2022a	74.7	48.2	19.4	54.5
DeiT 2022	70.4	40.9	12.8	48.4
LiVT 2023	73.6	56.4	41.0	60.9
LiVT + `Img2Img`^{L}	74.3	56.4	34.3	60.5
LiVT + `Img2Img`^{H}	73.8	56.4	45.3	61.6
LiVT + `Txt2Img`	**74.9**	55.6	48.3	62.2
LiVT + `GeNIe-Ada`	74.0	**56.9**	**52.7**	**63.1**

(S) in the beginning to target category (T) towards the end. However, somewhere between 0 and 1, X_r will undergo a rapid transition from S to T. To demonstrate this hypothesis empirically, in Figs. 5 and A7, we visualize pairs of source images and target categories with their respective `GeNIe` generated augmentations for different noise ratios r, along with their corresponding PCA-projected embedding scatter plots (on the far left). We extract embeddings for all the images using a DINOv2 ViT-G pretrained backbone, which we assume as an oracle model in identifying the right category. We observe that as r increases from 0.3 to 0.8, the images transition to embody more of the target category's semantics while preserving the contextual features of the source image. This transition of semantics can also be observed in the embedding plots (on the left) where they consistently shift from the proximity of the source image (blue star) to the target class's centroid (red cross) as the noise ratio r increases. The sparse distribution of points within $r = [0.4, 0.6]$ for the first and second images and $r = [0.2, 0.4]$ for the third image aligns with our intuition of a rapid transition from category S to T, thus empirically affirming our motivation behind `GeNIe-Ada`.

To further establish this, in Fig. 6, we demonstrate the efficacy of `GeNIe` in generating hard negatives at the decision boundaries of an SVM classifier, which is trained on the labelled support set of the few-shot tasks of *mini*-Imagenet, without any augmentations. We then plot source and target class probabilities ($P(Y_S|X_r)$ and $P(Y_T|X_r)$, respectively) of the generated augmentation samples X_r. For both $r = 0.6$ and 0.7, there is significant overlap between $P(Y_S|X_r)$ and $P(Y_T|X_r)$, making it difficult for the classifier to decide the correct class. On the right-hand-side, `GeNIe-Ada` automatically selects the best r resulting in the most overlap between the two distributions, thus offering the hardest negative sample among the considered r values (for more details see A.1). Note that a large overlap between distributions is not sufficient to call the generated samples hard negatives because they should also belong to the target category. This is, however, confirmed by the high Oracle accuracy in Table 5 (elaborated in detail in the following paragraph) which verifies that majority of the generated augmentation samples do belong to the target category.

Label consistency of the generated samples. The choice of noise ratio r is important in producing hard negative examples. In Table 5, we present the accuracy of the `GeNIe` model across various noise ratios, alongside the oracle accuracy, which is an ImageNet pre-trained DeiT-Base (Touvron et al., 2021b) classifier. We observe a decline in the label consistency of generated data (quantified by the performance of the oracle model) when decreasing the noise level. Reducing r also results in a degradation in the performance of the

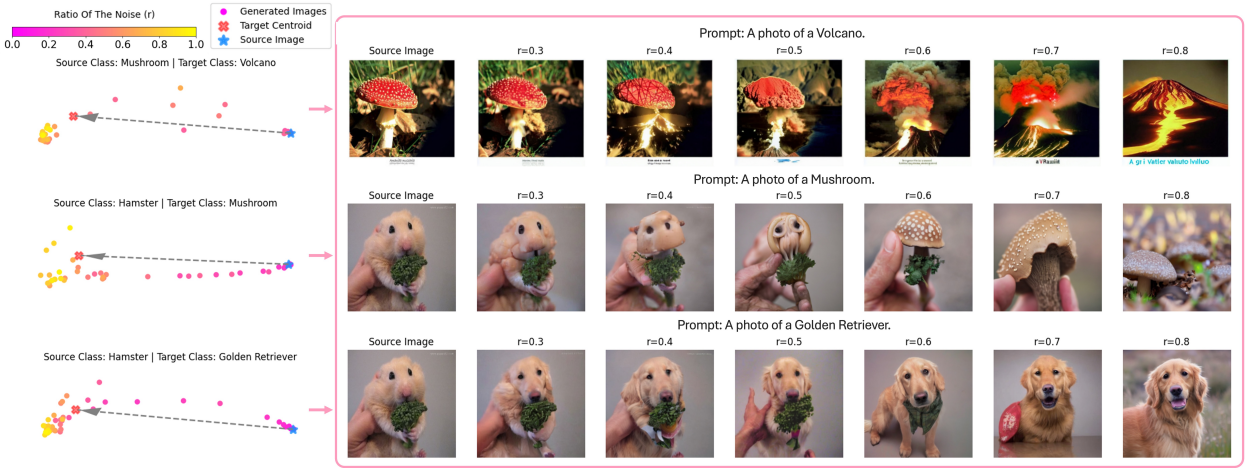

Figure 5: **Embedding visualizations of generative augmentations:** We pass all generative augmentations through DINOv2 ViT-G (serving as an oracle) to extract their corresponding embeddings and visualize them with PCA. As shown, the extent of semantic shifts varies based on both the source image and the target class.

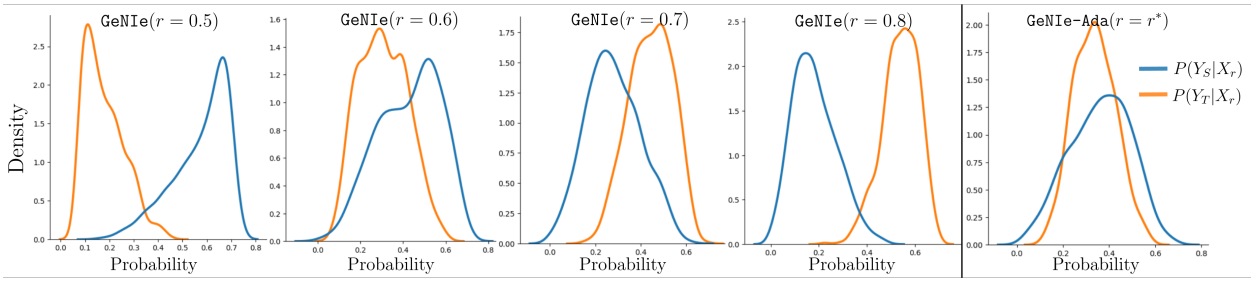

Figure 6: **Why `GeNIe` augmentations are challenging?** While deciding which class the generated augmentations (X_r) belong to is already difficult within $r = [0.6, 0.7]$ (due to high overlap between $P(Y_S|X_r)$ and $P(Y_T|X_r)$), `GeNIe-Ada` selects the best noise threshold (r^*) offering the hardest negative sample.

final few-shot model (87.2% → 77.6%) corroborating that an appropriate choice of r plays a crucial role. We investigate this further in the following paragraph.

Effect of Noise in `GeNIe`. We examine the impact of noise on the performance of the few-shot model in Table 5. Noise levels $r \in [0.7, 0.8]$ yield the best performance. Conversely, utilizing noise levels below 0.7 diminishes performance due to label inconsistency, as is demonstrated in Table 5 and Fig 5. As such, determining the appropriate noise level is pivotal for the performance of `GeNIe` to be able to generate challenging hard negatives while maintaining label consistency. An alternative approach to finding the optimal noise level involves using `GeNIe-Ada` to adaptively select the noise level for each source image and target class. As demonstrated in Tables 5 and 2, `GeNIe-Ada` matches or outperforms `GeNIe` with fixed noise levels.

Effect of Diffusion Models in `GeNIe`. We have tried experimenting with both smaller as well as more recent diffusion models. More specifically, we have used Stable Diffusion XL-Turbo to generate hard-negatives through `GeNIe` and `GeNIe-Ada`. Few-shot classification results on miniImagenet with these augmentations are shown in Table 5. The accuracies follow a similar trend to that of Table 1, where Stable Diffusion 1.5 was used to generate augmentations. `GeNIe-Ada` improves UniSiam's few-shot performance the most as compared to `GeNIe` with different noise ratios r, and even when compared to `Txt2Img`. This empirically indicates the robustness of `GeNIe` and `GeNIe-Ada` to different diffusion engines. Note that, Stable Diffusion XL-Turbo by default uses 4 steps for the sake of optimization, and to ensure we can have the right granularity for the choice of r we have set the number of steps to 10. That is already 5 times faster than the standard Stable Diffusion v1.5 with 50 steps. Our experiments with Stable Diffusion v3 (which is a totally different

Table 5: **Effect of Noise and Diffusion Models in GeNIe:** We use the same setting as in Table 1 to study the effect of the amount of noise. As expected (also shown in Fig 5), small noise results in worse accuracy since some generated images may be from the source category rather than the target one. For $r = 0.5$ only 73% of the generated data is from the target category. This behaviour is also shown in Fig. 2. Notably, reducing the noise level below 0.7 is associated with a decline in oracle accuracy and subsequent degradation in the performance of the final few-shot model. Note that the high oracle accuracy of GeNIe-Ada demonstrates its capability to adaptively select the noise level per source and target, ensuring semantic consistency with the intended target. To further demonstrate GeNIe's ability to generalize across different diffusion models, we replace the diffusion model with SD3 and SDXL-Turbo. The resulting accuracies follow a similar trend to those in Table 1, confirming GeNIe's advantage over Txt2Img across various diffusion models.

Method	Generative Model	Noise r=	ResNet-18 1-shot	ResNet-18 5-shot	ResNet-34 1-shot	ResNet-34 5-shot	ResNet-50 1-shot	ResNet-50 5-shot	Oracle Acc
Txt2Img	SD 1.5	-	74.1±0.6	84.6±0.5	75.4±0.6	85.5±0.5	76.4±0.6	86.5±0.4	-
GeNIe	SD 1.5	0.5	60.4±0.8	74.1±0.6	62.0±0.8	75.8±0.6	63.7±0.9	77.6±0.6	73.4±0.5
GeNIe	SD 1.5	0.6	69.7±0.7	80.7±0.5	71.1±0.7	82.2±0.5	72.1±0.7	82.8±0.5	85.8±0.4
GeNIe	SD 1.5	0.7	74.5±0.6	83.3±0.5	76.4±0.6	84.4±0.5	77.1±0.6	85.0±0.4	94.5±0.2
GeNIe	SD 1.5	0.8	75.5±0.6	85.4±0.4	77.1±0.6	86.3±0.4	77.3±0.6	87.2±0.4	98.2±0.1
GeNIe	SD 1.5	0.9	75.0±0.6	85.3±0.4	77.6±0.6	86.2±0.4	77.7±0.6	87.0±0.4	99.3±0.1
GeNIe-Ada	SD 1.5	Adaptive	76.8±0.6	85.9±0.4	78.5±0.6	86.6±0.4	78.6±0.6	87.9±0.4	98.9±0.2
Txt2Img	SDXL-Turbo	-	72.5±0.3	82.1±0.6	76.2±0.2	84.4±0.3	76.7±0.6	85.9±0.5	-
GeNIe	SDXL-Turbo	0.5	61.2±0.5	73.5±0.2	61.5±0.2	74.9±0.3	63.1±0.2	76.5±0.6	-
GeNIe	SDXL-Turbo	0.6	70.2±0.2	79.3±0.4	71.2±0.7	81.4±0.6	73.2±0.2	82.4±0.5	-
GeNIe	SDXL-Turbo	0.7	73.1±0.3	83.5±0.5	76.1±0.6	85.3±0.4	77.2±0.6	84.2±0.4	-
GeNIe	SDXL-Turbo	0.8	74.2±0.3	85.1±0.3	76.9±0.4	85.5±0.5	78.7±0.6	87.7±0.4	-
GeNIe	SDXL-Turbo	0.9	73.9±0.4	84.9±0.7	76.6±0.7	84.2±0.6	78.1±0.5	87.0±0.4	-
GeNIe-Ada	SDXL-Turbo	Adaptive	75.1±0.3	87.1±0.8	78.9±0.5	85.2±0.5	79.0±0.6	88.6±0.2	-
Txt2Img	SD 3	-	73.6±1.7	82.9±1.2	76.7±1.5	85.5±1.3	77.2±1.9	85.0±1.2	-
GeNIe	SD 3	0.5	62.0±1.2	72.9±1.1	62.5±0.9	73.9±1.0	64.1±0.5	76.1±1.9	-
GeNIe	SD 3	0.6	70.8±1.5	79.1±1.9	71.8±1.2	82.1±1.3	74.1±1.5	83.4±1.8	-
GeNIe	SD 3	0.7	74.6±0.8	84.5±1.2	76.5±1.9	86.2±1.6	78.5±1.9	84.0±1.1	-
GeNIe	SD 3	0.8	75.9±1.2	86.3±1.7	77.8±1.9	85.5±1.9	79.2±1.7	88.3±1.9	-
GeNIe	SD 3	0.9	75.1±0.5	85.2±1.2	78.1±1.3	86.2±1.2	77.1±1.9	88.9±0.8	-
GeNIe-Ada	SD 3	Adaptive	76.8±1.3	87.5±1.5	78.9±1.3	87.7±1.5	79.1±1.4	89.5±1.0	-

model with a Transformers backbone) also in Table 5 also convey the same message. As such, we believe our approach is generalizable across different diffusion models.

5 Concluding Remarks

GeNIe, for the first time to our knowledge, combines contradictory sources of information (a source image, and a different target category prompt) through a noise adjustment strategy into a conditional latent diffusion model to generate challenging augmentations, which can serve as hard negatives.

Limitation. The required time to create augmentations through GeNIe is on par with any typical diffusion-based competitors (Azizi et al., 2023; He et al., 2022b); however, this is naturally slower than traditional augmentation techniques (Yun et al., 2019a; Zhang et al., 2018). This is not a bottleneck in offline augmentation strategies, but can be considered a limiting factor in real-time scenarios. Recent studies are already mitigating this through advancements in diffusion model efficiency (Sauer et al., 2023; Meng et al., 2023; Liu et al., 2023). Another challenge present in any generative AI-based augmentation technique is the domain shift between the distribution of training data and the downstream context they might be used for augmentation. A possible remedy is to fine-tune the diffusion backbone on a rather small dataset from the downstream task.

Broader Impact. GeNIe can have a significant impact when it comes to generating challenging augmentations and thus enhancing downstream tasks beyond classification. Like any other generative model, GeNIe can also introduce inherent biases stemming from the training data used to build its diffusion backbone, which can reflect and amplify societal prejudices or inaccuracies. Therefore, it is crucial to carefully mitigate potential biases in generative models such as GeNIe to ensure a fair and ethical deployment of deep learning systems.

References

Arman Afrasiyabi, Jean-François Lalonde, and Christian Gagné. Associative alignment for few-shot image classification. In *ECCV*, 2019.

Jean-Baptiste Alayrac, Jeff Donahue, Pauline Luc, Antoine Miech, Iain Barr, Yana Hasson, Karel Lenc, Arthur Mensch, Katie Millican, Malcolm Reynolds, Roman Ring, Eliza Rutherford, Serkan Cabi, Tengda Han, Zhitao Gong, Sina Samangooei, Marianne Monteiro, Jacob Menick, Sebastian Borgeaud, Andrew Brock, Aida Nematzadeh, Sahand Sharifzadeh, Mikolaj Binkowski, Ricardo Barreira, Oriol Vinyals, Andrew Zisserman, and Karen Simonyan. Flamingo: a visual language model for few-shot learning, 2022.

Antreas Antoniou and Amos Storkey. Assume, augment and learn: Unsupervised few-shot meta-learning via random labels and data augmentation. *arxiv:1902.09884*, 2019.

Shekoofeh Azizi, Simon Kornblith, Chitwan Saharia, Mohammad Norouzi, and David J. Fleet. Synthetic data from diffusion models improves imagenet classification, 2023.

Lukas Bossard, Matthieu Guillaumin, and Luc Van Gool. Food-101 – mining discriminative components with random forests. In *European Conference on Computer Vision*, 2014.

Jiarui Cai, Yizhou Wang, Jenq-Neng Hwang, et al. Ace: Ally complementary experts for solving long-tailed recognition in one-shot. In *ICCV*, pp. 112–121, 2021.

Kaidi Cao, Colin Wei, Adrien Gaidon, Nikos Arechiga, and Tengyu Ma. Learning imbalanced datasets with label-distribution-aware margin loss. *NeurIPS*, 32, 2019.

Atoosa Chegini and Soheil Feizi. Identifying and mitigating model failures through few-shot clip-aided diffusion generation. *arXiv preprint arXiv:2312.05464*, 2023.

Ting Chen, Simon Kornblith, Mohammad Norouzi, and Geoffrey Hinton. A simple framework for contrastive learning of visual representations. In *ICML*, 2020.

Wei-Yu Chen, Yen-Cheng Liu, Zsolt Kira, Yu-Chiang Frank Wang, and Jia-Bin Huang. A closer look at few-shot classification. In *ICLR*, 2019a.

Wentao Chen, Chenyang Si, Wei Wang, Liang Wang, Zilei Wang, and Tieniu Tan. Few-shot learning with part discovery and augmentation from unlabeled images. *arXiv preprint arXiv:2105.11874*, 2021.

Xinlei Chen and Kaiming He. Exploring simple siamese representation learning. In *CVPR*, 2021.

Zhengyu Chen, Jixie Ge, Heshen Zhan, Siteng Huang, and Donglin Wang. Pareto self-supervised training for few-shot learning. In *CVPR*, 2021.

Zitian Chen, Yanwei Fu, Yu-Xiong Wang, Lin Ma, Wei Liu, and Martial Hebert. Image deformation meta-networks for one-shot learning. In *CVPR*, 2019b.

Ekin D. Cubuk, Barret Zoph, Dandelion Mane, Vijay Vasudevan, and Quoc V. Le. Autoaugment: Learning augmentation policies from data, 2019a.

Ekin D. Cubuk, Barret Zoph, Jonathon Shlens, and Quoc V. Le. Randaugment: Practical automated data augmentation with a reduced search space, 2019b.

Ekin Dogus Cubuk, Barret Zoph, Jon Shlens, and Quoc Le. Randaugment: Practical automated data augmentation with a reduced search space. In H. Larochelle, M. Ranzato, R. Hadsell, M.F. Balcan, and H. Lin (eds.), *Advances in Neural Information Processing Systems*, volume 33, pp. 18613–18624. Curran Associates, Inc., 2020. URL https://proceedings.neurips.cc/paper/2020/file/d85b63ef0ccb114d0a3bb7b7d808028f-Paper.pdf.

Jiequan Cui, Zhisheng Zhong, Shu Liu, Bei Yu, and Jiaya Jia. Parametric contrastive learning. In *ICCV*, pp. 715–724, 2021a.

Jiequan Cui, Zhisheng Zhong, Shu Liu, Bei Yu, and Jiaya Jia. Parametric contrastive learning. In *Proceedings of the IEEE/CVF international conference on computer vision*, pp. 715–724, 2021b.

Jiequan Cui, Shu Liu, Zhuotao Tian, Zhisheng Zhong, and Jiaya Jia. Reslt: Residual learning for long-tailed recognition. *IEEE transactions on pattern analysis and machine intelligence*, 45(3):3695–3706, 2022.

Yin Cui, Menglin Jia, Tsung-Yi Lin, Yang Song, and Serge Belongie. Class-balanced loss based on effective number of samples. In *CVPR*, pp. 9268–9277, 2019.

Jia Deng, Wei Dong, Richard Socher, Li-Jia Li, Kai Li, and Li Fei-Fei. Imagenet: A large-scale hierarchical image database. In *2009 IEEE conference on computer vision and pattern recognition*, pp. 248–255. Ieee, 2009.

Mucong Ding, Bang An, Yuancheng Xu, Anirudh Satheesh, and Furong Huang. SAFLEX: Self-adaptive augmentation via feature label extrapolation. In *The Twelfth International Conference on Learning Representations*, 2024. URL https://openreview.net/forum?id=qL6brrBDk2.

Alexey Dosovitskiy, Lucas Beyer, Alexander Kolesnikov, Dirk Weissenborn, Xiaohua Zhai, Thomas Unterthiner, Mostafa Dehghani, Matthias Minderer, Georg Heigold, Sylvain Gelly, Jakob Uszkoreit, and Neil Houlsby. An image is worth 16x16 words: Transformers for image recognition at scale. In *ICLR*, 2021.

Lisa Dunlap, Clara Mohri, Han Zhang, Devin Guillory, Trevor Darrell, Joseph E. Gonzalez, Anna Rohrbach, and Aditi Raghunathan. Using language to extend to unseen domains. *International Conference on Learning Representations (ICLR)*, 2023a.

Lisa Dunlap, Alyssa Umino, Han Zhang, Jiezhi Yang, Joseph E. Gonzalez, and Trevor Darrell. Diversify your vision datasets with automatic diffusion-based augmentation, 2023b.

Nikita Dvornik, Julien Mairal, and Cordelia Schmid. Diversity with cooperation: Ensemble methods for few-shot classification. In *ICCV*, 2019.

Chun-Mei Feng, Kai Yu, Yong Liu, Salman Khan, and Wangmeng Zuo. Diverse data augmentation with diffusions for effective test-time prompt tuning, 2023.

Chelsea Finn, Pieter Abbeel, and Sergey Levine. Model-agnostic meta-learning for fast adaptation of deep networks. In *Proceedings of the 34th International Conference on Machine Learning*, pp. 1126–1135, 2017.

Maayan Frid-Adar, Idit Diamant, Eyal Klang, Michal Amitai, Jacob Goldberger, and Hayit Greenspan. Gan-based synthetic medical image augmentation for increased cnn performance in liver lesion classification. *Neurocomputing*, 2018.

Rinon Gal, Yuval Alaluf, Yuval Atzmon, Or Patashnik, Amit H Bermano, Gal Chechik, and Daniel Cohen-Or. An image is worth one word: Personalizing text-to-image generation using textual inversion. *arXiv preprint arXiv:2208.01618*, 2022a.

Rinon Gal, Yuval Alaluf, Yuval Atzmon, Or Patashnik, Amit H. Bermano, Gal Chechik, and Daniel Cohen-Or. An image is worth one word: Personalizing text-to-image generation using textual inversion, 2022b. URL https://arxiv.org/abs/2208.01618.

Rinon Gal, Yuval Alaluf, Yuval Atzmon, Or Patashnik, Amit H. Bermano, Gal Chechik, and Daniel Cohen-Or. An image is worth one word: Personalizing text-to-image generation using textual inversion, 2022c. URL https://arxiv.org/abs/2208.01618.

Alexandros Graikos, Srikar Yellapragada, and Dimitris Samaras. Conditional generation from pre-trained diffusion models using denoiser representations. In *34th British Machine Vision Conference 2023, BMVC 2023, Aberdeen, UK, November 20-24, 2023*. BMVA, 2023a. URL https://papers.bmvc2023.org/0478.pdf.

Alexandros Graikos, Srikar Yellapragada, and Dimitris Samaras. Conditional generation from unconditional diffusion models using denoiser representations. *arXiv preprint arXiv:2306.01900*, 2023b.

Kaiming He, Xinlei Chen, Saining Xie, Yanghao Li, Piotr Dollár, and Ross Girshick. Masked autoencoders are scalable vision learners, 2021.

Kaiming He, Xinlei Chen, Saining Xie, Yanghao Li, Piotr Dollár, and Ross B. Girshick. Masked autoencoders are scalable vision learners. In *CVPR*, pp. 15979–15988. IEEE, 2022a.

Ruifei He, Shuyang Sun, Xin Yu, Chuhui Xue, Wenqing Zhang, Philip Torr, Song Bai, and Xiaojuan Qi. Is synthetic data from generative models ready for image recognition? *arXiv preprint arXiv:2210.07574*, 2022b.

Reyhane Askari Hemmat, Mohammad Pezeshki, Florian Bordes, Michal Drozdzal, and Adriana Romero-Soriano. Feedback-guided data synthesis for imbalanced classification, 2023.

Dan Hendrycks, Norman Mu, Ekin D. Cubuk, Barret Zoph, Justin Gilmer, and Balaji Lakshminarayanan. AugMix: A simple data processing method to improve robustness and uncertainty. *Proceedings of the International Conference on Learning Representations (ICLR)*, 2020.

Yan Hong, Jianfu Zhang, Zhongyi Sun, and Ke Yan. Safa: Sample-adaptive feature augmentation for long-tailed image classification. In *ECCV*, 2022.

Kyle Hsu, Sergey Levine, and Chelsea Finn. Unsupervised learning via meta-learning. In *ICLR*, 2018.

Wentao Hu, Xiurong Jiang, Jiarun Liu, Yuqi Yang, and Hui Tian. Meta-dm: Applications of diffusion models on few-shot learning, 2023.

Sheng-Wei Huang, Che-Tsung Lin, Shu-Ping Chen, Yen-Yi Wu an Po-Hao Hsu, and Shang-Hong Lai. Auggan: Cross domain adaptation with gan-based data augmentation. *European Conference on Computer Vision*, 2018.

Saachi Jain, Hannah Lawrence, Ankur Moitra, and Aleksander Madry. Distilling model failures as directions in latent space. In *ArXiv preprint arXiv:2206.14754*, 2022.

Huiwon Jang, Hankook Lee, and Jinwoo Shin. Unsupervised meta-learning via few-shot pseudo-supervised contrastive learning. In *The Eleventh International Conference on Learning Representations*, 2022.

Bingyi Kang, Saining Xie, Marcus Rohrbach, Zhicheng Yan, Albert Gordo, Jiashi Feng, and Yannis Kalantidis. Decoupling representation and classifier for long-tailed recognition. *arXiv preprint arXiv:1910.09217*, 2019.

Bingyi Kang, Saining Xie, Marcus Rohrbach, Zhicheng Yan, Albert Gordo, Jiashi Feng, and Yannis Kalantidis. Decoupling representation and classifier for long-tailed recognition. In *ICLR*, 2020.

Siavash Khodadadeh, Ladislau Boloni, and Mubarak Shah. Unsupervised meta-learning for few-shot image classification. In *NeurIPS*, 2019.

Jang-Hyun Kim, Wonho Choo, and Hyun Oh Song. Puzzle mix: Exploiting saliency and local statistics for optimal mixup. In *International Conference on Machine Learning*, pp. 5275–5285. PMLR, 2020.

Jonathan Krause, Michael Stark, Jia Deng, and Li Fei-Fei. 3D object representations for fine-grained categorization. In *Workshop on 3D Representation and Recognition*, Sydney, Australia, 2013.

Alexander C. Li, Mihir Prabhudesai, Shivam Duggal, Ellis Brown, and Deepak Pathak. Your diffusion model is secretly a zero-shot classifier, 2023.

Bolian Li, Zongbo Han, Haining Li, Huazhu Fu, and Changqing Zhang. Trustworthy long-tailed classification. In *CVPR*, pp. 6970–6979, 2022a.

Daiqing Li, Huan Ling, Seung Wook Kim, Karsten Kreis, Adela Barriuso, Sanja Fidler, and Antonio Torralba. Bigdatasetgan: Synthesizing imagenet with pixel-wise annotations, 2022b.

Jun Li, Zichang Tan, Jun Wan, Zhen Lei, and Guodong Guo. Nested collaborative learning for long-tailed visual recognition. In *CVPR*, pp. 6949–6958, 2022c.

Junnan Li, Dongxu Li, Caiming Xiong, and Steven Hoi. Blip: Bootstrapping language-image pre-training for unified vision-language understanding and generation, 2022d.

Kai Li, Yulun Zhang, Kunpeng Li, and Yun Fu. Adversarial feature hallucination networks for few-shot learning. In *CVPR*, 2020.

Mengke Li, Yiu-ming Cheung, Yang Lu, et al. Long-tailed visual recognition via gaussian clouded logit adjustment. In *CVPR*, pp. 6929–6938, 2022e.

Tianhong Li, Peng Cao, Yuan Yuan, Lijie Fan, Yuzhe Yang, Rogerio S Feris, Piotr Indyk, and Dina Katabi. Targeted supervised contrastive learning for long-tailed recognition. In *CVPR*, pp. 6918–6928, 2022f.

Bin Liu, Yue Cao, Yutong Lin, Qi Li, Zheng Zhang, Mingsheng Long, and Han Hu. Negative margin matters: Understanding margin in few-shot classification. In *ECCV*, 2020.

Xingchao Liu, Xiwen Zhang, Jianzhu Ma, Jian Peng, et al. Instaflow: One step is enough for high-quality diffusion-based text-to-image generation. In *The Twelfth International Conference on Learning Representations*, 2023.

Zicheng Liu, Siyuan Li, Di Wu, Zihan Liu, Zhiyuan Chen, Lirong Wu, and Stan Z Li. Automix: Unveiling the power of mixup for stronger classifiers. In *Computer Vision–ECCV 2022: 17th European Conference, Tel Aviv, Israel, October 23–27, 2022, Proceedings, Part XXIV*, pp. 441–458. Springer, 2022.

Ziwei Liu, Zhongqi Miao, Xiaohang Zhan, Jiayun Wang, Boqing Gong, and Stella X. Yu. Large-scale long-tailed recognition in an open world. In *CVPR*, 2019.

Yuning Lu, Liangjian Wen, Jianzhuang Liu, Yajing Liu, and Xinmei Tian. Self-supervision can be a good few-shot learner. In *European Conference on Computer Vision*, pp. 740–758. Springer, 2022.

Xue-Jing Luo, Shuo Wang, Zongwei Wu, Christos Sakaridis, Yun Cheng, Deng-Ping Fan, and Luc Van Gool. Camdiff: Camouflage image augmentation via diffusion model, 2023.

Lorenzo Luzi, Ali Siahkoohi, Paul M Mayer, Josue Casco-Rodriguez, and Richard Baraniuk. Boomerang: Local sampling on image manifolds using diffusion models, 2022.

Subhransu Maji, Esa Rahtu, Juho Kannala, Matthew B. Blaschko, and Andrea Vedaldi. Fine-grained visual classification of aircraft. *arXiv preprint arXiv:1306.5151*, 2013.

Jiayuan Mao, Tete Xiao, Yuning Jiang, and Zhimin Cao. What can help pedestrian detection?, 2017.

Carlos Medina, Arnout Devos, and Matthias Grossglauser. Self-supervised prototypical transfer learning for few-shot classification. In *ICMLW*, 2020.

Chenlin Meng, Yutong He, Yang Song, Jiaming Song, Jiajun Wu, Jun-Yan Zhu, and Stefano Ermon. Sdedit: Guided image synthesis and editing with stochastic differential equations. *arXiv preprint arXiv:2108.01073*, 2021.

Chenlin Meng, Robin Rombach, Ruiqi Gao, Diederik Kingma, Stefano Ermon, Jonathan Ho, and Tim Salimans. On distillation of guided diffusion models. In *Proceedings of the IEEE/CVF Conference on Computer Vision and Pattern Recognition*, pp. 14297–14306, 2023.

Aditya Krishna Menon, Sadeep Jayasumana, Ankit Singh Rawat, Himanshu Jain, Andreas Veit, and Sanjiv Kumar. Long-tail learning via logit adjustment. In *ICLR*, 2021.

Maxime Oquab, Timothée Darcet, Théo Moutakanni, Huy Vo, Marc Szafraniec, Vasil Khalidov, Pierre Fernandez, Daniel Haziza, Francisco Massa, Alaaeldin El-Nouby, Mahmoud Assran, Nicolas Ballas, Wojciech Galuba, Russell Howes, Po-Yao Huang, Shang-Wen Li, Ishan Misra, Michael Rabbat, Vasu Sharma, Gabriel Synnaeve, Hu Xu, Hervé Jegou, Julien Mairal, Patrick Labatut, Armand Joulin, and Piotr Bojanowski. Dinov2: Learning robust visual features without supervision, 2023.

William Peebles, Jun-Yan Zhu, Richard Zhang, Antonio Torralba, Alexei Efros, and Eli Shechtman. Gan-supervised dense visual alignment. In *CVPR*, 2022.

Suzanne Petryk, Lisa Dunlap, Keyan Nasseri, Joseph Gonzalez, Trevor Darrell, and Anna Rohrbach. On guiding visual attention with language specification. In *Conference on Computer Vision and Pattern Recognition (CVPR)*, 2022. doi: 10.48550/ARXIV.2202.08926. URL https://arxiv.org/abs/2202.08926.

Viraj Prabhu, Sriram Yenamandra, Prithvijit Chattopadhyay, and Judy Hoffman. Lance: Stress-testing visual models by generating language-guided counterfactual images. *Advances in Neural Information Processing Systems*, 36, 2024.

Siyuan Qiao, Chenxi Liu, Wei Shen, and Alan Yuille. Few-shot image recognition by predicting parameters from activations. In *CVPR*, 2018.

Tiexin Qin, Wenbin Li, Yinghuan Shi, and Gao Yang. Unsupervised few-shot learning via distribution shift-based augmentation. *arxiv:2004.05805*, 2020.

Alec Radford, Jong Wook Kim, Chris Hallacy, Aditya Ramesh, Gabriel Goh, Sandhini Agarwal, Girish Sastry, Amanda Askell, Pamela Mishkin, Jack Clark, Gretchen Krueger, and Ilya Sutskever. Learning transferable visual models from natural language supervision. In *ICML*, 2021.

Aditya Ramesh, Mikhail Pavlov, Gabriel Goh, Scott Gray, Chelsea Voss, Alec Radford, Mark Chen, and Ilya Sutskever. Zero-shot text-to-image generation. In *ICML*, 2021.

Aditya Ramesh, Prafulla Dhariwal, Alex Nichol, Casey Chu, and Mark Chen. Hierarchical text-conditional image generation with clip latents. *arXiv preprint arXiv:2204.06125*, 1(2):3, 2022.

Sachin Ravi and H. Larochelle. Optimization as a model for few-shot learning. In *ICLR*, 2017.

Mengye Ren, Sachin Ravi, Eleni Triantafillou, Jake Snell, Kevin Swersky, Josh B. Tenenbaum, Hugo Larochelle, and Richard S. Zemel. Meta-learning for semi-supervised few-shot classification. In *International Conference on Learning Representations*, 2018. URL https://openreview.net/forum?id=HJcSzz-CZ.

Robin Rombach, Andreas Blattmann, Dominik Lorenz, Patrick Esser, and Björn Ommer. High-resolution image synthesis with latent diffusion models, 2021.

Robin Rombach, Andreas Blattmann, Dominik Lorenz, Patrick Esser, and BjÃ¶rn Ommer. High-resolution image synthesis with latent diffusion models. In *CVPR*, 2022.

Aniket Roy, Anshul Shah, Ketul Shah, Anirban Roy, and Rama Chellappa. Cap2aug: Caption guided image to image data augmentation, 2023.

Chitwan Saharia, William Chan, Saurabh Saxena, Lala Li, Jay Whang, Emily L Denton, Kamyar Ghasemipour, Raphael Gontijo Lopes, Burcu Karagol Ayan, Tim Salimans, et al. Photorealistic text-to-image diffusion models with deep language understanding. *Advances in Neural Information Processing Systems*, 35:36479–36494, 2022.

Dvir Samuel and Gal Chechik. Distributional robustness loss for long-tail learning. In *ICCV*, 2021.

Swami Sankaranarayanan, Yogesh Balaji, Carlos Domingo Castillo, and Rama Chellappa. Generate to adapt: Aligning domains using generative adversarial networks. *Conference on Computer Vision and Pattern Recognition (CVPR)*, 2018.

Axel Sauer, Dominik Lorenz, Andreas Blattmann, and Robin Rombach. Adversarial diffusion distillation. *arXiv preprint arXiv:2311.17042*, 2023.

Viktoriia Sharmanska, Lisa Anne Hendricks, Trevor Darrell, and Novi Quadrianto. Contrastive examples for addressing the tyranny of the majority. *CoRR*, abs/2004.06524, 2020. URL https://arxiv.org/abs/2004.06524.

Jordan Shipard, Arnold Wiliem, Kien Nguyen Thanh, Wei Xiang, and Clinton Fookes. Boosting zero-shot classification with synthetic data diversity via stable diffusion. *arXiv preprint arXiv:2302.03298*, 2023.

Ojas Kishorkumar Shirekar, Anuj Singh, and Hadi Jamali-Rad. Self-attention message passing for contrastive few-shot learning. In *Proceedings of the IEEE/CVF Winter Conference on Applications of Computer Vision (WACV)*, pp. 5426–5436, January 2023.

Connor Shorten and Taghi M Khoshgoftaar. A survey on image data augmentation for deep learning. *Journal of big data*, 6(1):1–48, 2019.

Anuj Rajeeva Singh and Hadi Jamali-Rad. Transductive decoupled variational inference for few-shot classification. *Transactions on Machine Learning Research*, 2023. ISSN 2835-8856. URL https://openreview.net/forum?id=bomdTc9HyL.

Jake Snell, Kevin Swersky, and Richard Zemel. Prototypical networks for few-shot learning. In *Advances in Neural Information Processing Systems*, 2017.

Jong-Chyi Su, Subhransu Maji, and Bharath Hariharan. When does self-supervision improve few-shot learning? In *ECCV*, 2020.

Flood Sung, Yongxin Yang, Li Zhang, Tao Xiang, Philip H.S. Torr, and Timothy M. Hospedales. Learning to compare: Relation network for few-shot learning. In *CVPR*, 2018.

Kaihua Tang, Jianqiang Huang, and Hanwang Zhang. Long-tailed classification by keeping the good and removing the bad momentum causal effect. *NeurIPS*, 33:1513–1524, 2020.

Kowshik Thopalli, Rakshith Subramanyam, Pavan Turaga, and Jayaraman J. Thiagarajan. Target-aware generative augmentations for single-shot adaptation. In *Proceedings of the 40th International Conference on Machine Learning*, ICML'23. JMLR.org, 2023.

Changyao Tian, Wenhai Wang, Xizhou Zhu, Jifeng Dai, and Yu Qiao. Vl-ltr: Learning class-wise visual-linguistic representation for long-tailed visual recognition. In *ECCV 2022*, 2022.

Yonglong Tian, Lijie Fan, Phillip Isola, Huiwen Chang, and Dilip Krishnan. Stablerep: Synthetic images from text-to-image models make strong visual representation learners, 2023. URL https://arxiv.org/abs/2306.00984.

Hugo Touvron, Matthieu Cord, Matthijs Douze, Francisco Massa, Alexandre Sablayrolles, and Hervé Jégou. Training data-efficient image transformers & distillation through attention. In *International Conference on Machine Learning (ICML)*, 2021a.

Hugo Touvron, Matthieu Cord, Matthijs Douze, Francisco Massa, Alexandre Sablayrolles, and Hervé Jégou. Training data-efficient image transformers and distillation through attention, 2021b.

Hugo Touvron, Matthieu Cord, and Hervé Jégou. Deit iii: Revenge of the vit. In *ECCV*, 2022.

Brandon Trabucco, Kyle Doherty, Max A Gurinas, and Ruslan Salakhutdinov. Effective data augmentation with diffusion models. In *The Twelfth International Conference on Learning Representations*, 2024. URL https://openreview.net/forum?id=ZWzUA9zeAg.

Nontawat Tritrong, Pitchaporn Rewatbowornwong, and Supasorn Suwajanakorn. Repurposing gans for one-shot semantic part segmentation. In *IEEE Conference on Computer Vision and Pattern Recognition (CVPR)*, 2021.

Catherine Wah, Steve Branson, Peter Welinder, Pietro Perona, and Serge Belongie. The caltech-ucsd birds-200-2011 dataset, 2011.

Haoqing Wang and Zhi-Hong Deng. Contrastive prototypical network with wasserstein confidence penalty. In *European Conference on Computer Vision*, pp. 665–682. Springer, 2022.

Hualiang Wang, Siming Fu, Xiaoxuan He, Hangxiang Fang, Zuozhu Liu, and Haoji Hu. Towards calibrated hyper-sphere representation via distribution overlap coefficient for long-tailed learning. In *ECCV*, 2022.

Xudong Wang, Long Lian, Zhongqi Miao, Ziwei Liu, and Stella X. Yu. Long-tailed recognition by routing diverse distribution-aware experts. In *ICLR*. OpenReview.net, 2021.

Yue Xu, Yong-Lu Li, Jiefeng Li, and Cewu Lu. Constructing balance from imbalance for long-tailed image recognition. In *ECCV*, pp. 38–56. Springer, 2022.

Zhengzhuo Xu, Ruikang Liu, Shuo Yang, Zenghao Chai, and Chun Yuan. Learning imbalanced data with vision transformers, 2023.

Hong Xuan, Abby Stylianou, Xiaotong Liu, and Robert Pless. Hard negative examples are hard, but useful, 2021.

Han-Jia Ye, Hexiang Hu, De-Chuan Zhan, and Fei Sha. Few-shot learning via embedding adaptation with set-to-set functions. In *CVPR*, 2020.

Sangdoo Yun, Dongyoon Han, Seong Joon Oh, Sanghyuk Chun, Junsuk Choe, and Youngjoon Yoo. Cutmix: Regularization strategy to train strong classifiers with localizable features. In *ICCV*, pp. 6023–6032, 2019a.

Sangdoo Yun, Dongyoon Han, Seong Joon Oh, Sanghyuk Chun, Junsuk Choe, and Youngjoon Yoo. Cutmix: Regularization strategy to train strong classifiers with localizable features. In *International Conference on Computer Vision (ICCV)*, 2019b.

Hongyi Zhang, Moustapha Cisse, Yann N. Dauphin, and David Lopez-Paz. mixup: Beyond empirical risk minimization. In *ICLR*, 2018.

Songyang Zhang, Zeming Li, Shipeng Yan, Xuming He, and Jian Sun. Distribution alignment: A unified framework for long-tail visual recognition. In *CVPR*, pp. 2361–2370, 2021a.

Yifan Zhang, Bryan Hooi, Lanqing Hong, and Jiashi Feng. Test-agnostic long-tailed recognition by test-time aggregating diverse experts with self-supervision. *arXiv preprint arXiv:2107.09249*, 2021b.

Yuxuan Zhang, Huan Ling, Jun Gao, Kangxue Yin, Jean-Francois Lafleche, Adela Barriuso, Antonio Torralba, and Sanja Fidler. Datasetgan: Efficient labeled data factory with minimal human effort. In *CVPR*, 2021c.

Zhisheng Zhong, Jiequan Cui, Shu Liu, and Jiaya Jia. Improving calibration for long-tailed recognition. In *CVPR*, pp. 16489–16498. Computer Vision Foundation / IEEE, 2021.

Ziqi Zhou, Xi Qiu, Jiangtao Xie, Jianan Wu, and Chi Zhang. Binocular mutual learning for improving few-shot classification. In *ICCV*, 2021.

Jianggang Zhu, Zheng Wang, Jingjing Chen, Yi-Ping Phoebe Chen, and Yu-Gang Jiang. Balanced contrastive learning for long-tailed visual recognition. In *CVPR*, pp. 6908–6917, 2022.

A Appendix

A.1 Analyzing GeNIe, GeNIe-Ada's Class-Probabilities

The core aim of GeNIe and GeNIe-Ada is to address the failure modes of a classifier by generating *challenging* samples located near the decision boundary of each class pair, which facilitates the learning process in effectively enhancing the decision boundary between classes. As summarized in Table 5 and illustrated in Fig. 5, we have empirically corroborated that GeNIe and GeNIe-Ada can respectively produce samples X_r, X_{r^*} that are negative with respect to the source image X_S, while semantically belonging to the class T. To further analyze the effectiveness of GeNIe and GeNIe-Ada, we compare the

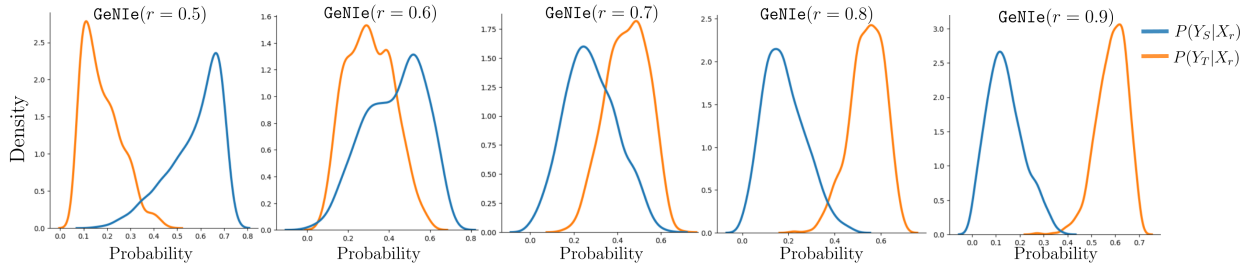

Figure A1: $P(Y_S|X_r)$ and $P(Y_T|X_r)$ for $r \in \{0.5, 0.6, 0.7, 0.8, 0.9\}$. On average, the classifier confidently predicts the source class more than the target class for X_r for $r = 0.5$, and vice-versa for $r = 0.8, 0.9$. However, for $r = 0.6, 0.7$, the classifier struggles to classify X_r, indicating that the augmented samples are located closer to the decision boundary.

source class-probabilities $P(Y_S|X_r)$ and target-class probabilities $P(Y_S|X_r)$ of augmented samples X_r. To compute these class probabilities, we first fit an SVM classifier (as followed in UniSiam (Lu et al., 2022)) only on the labelled support set embeddings of each episode in the *mini*Imagenet test dataset. Then, we perform inference using each episode's SVM classifier on its respective X_r's and extract its class probabilities of belonging to its source class S and target class T. These per augmentation-sample source and target class probabilities are then averaged for each episode for each $r \in \{0.5, 0.6, 0.7, 0.8, 0.9\}$ in the case of GeNIe and for the optimal $r = r^*$ per sample in the case of GeNIe-Ada, plotted as density plots in Fig. A1, Fig. A2, respectively. Fig. A1 illustrates that $P(Y_S|X_r)$ and $P(Y_T|X_r)$ have significant overlap in the case of $r \in \{0.6, 0.7\}$ indicating class-confusion for X_r.

Furthermore, Fig. A2 illustrates that when using the optimal $r = r^*$ found by GeNIe-Ada per sample, $P(Y_S|X_r)$ and $P(Y_T|X_r)$ significantly overlap around probability scores of $0.2 - 0.45$, indicating class confusion for GeNIe-Ada augmentations. This corroborates with our analysis in Section 4.4, Table 5 and additionally empirically proves that the augmented samples generated by GeNIe for $r \in \{0.6, 0.7\}$ and GeNIe-Ada for $r = r^*$ are actually located near the decision boundary of each class pair.

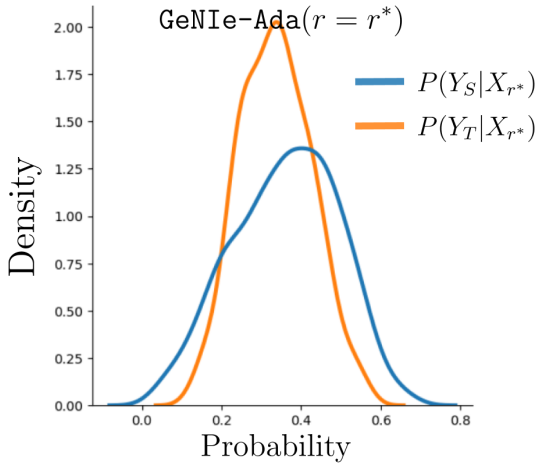

Figure A2: Significant overlap between $P(Y_S|X_{r^*})$ and $P(Y_T|X_{r^*})$ indicates high class-confusion for augmented samples generated by GeNIe-Ada.

A.2 Independence of Generated Augmentations from Downstream Test Sets

Here we analyzed whether the augmented samples generated by GeNIe using the diffusion model overlap with the test set of the downstream task. To set the stage, we extracted the latent embeddings corresponding to the train set (i.e., support), test set (i.e., query), and augmentations generated by GeNIe. Fig A3 illustrates the distribution of distances between train-test and augmentation-test pairs across 600 episodes. Notably, the mean distance of augmentation-test pairs is higher than that of train-test pairs, indicating that the

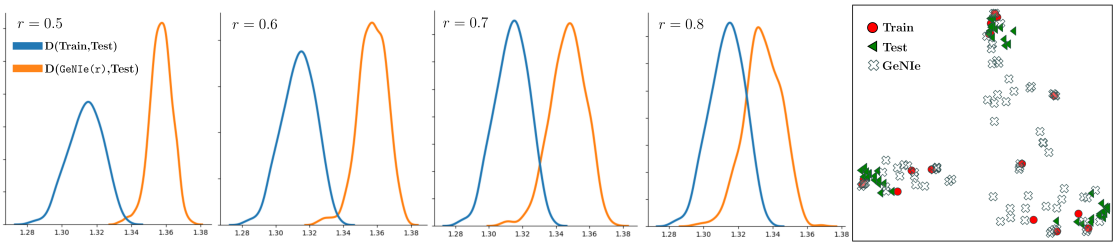

Figure A3: Comparison of embedding distributions and UMAP visualization for train, test, and GeNIe-augmented samples.

augmented samples are distinct from the test set. This observation aligns with the fundamental assumption of train and test sets being mutually exclusive. Additionally, Fig A3 provides further evidence through a UMAP embedding plot of a randomly selected episode, where the embeddings of train, test, and augmented samples are visualized. The plot reveals clear separations between the test set and augmented samples, further confirming that the augmented samples do not overlap with or resemble the test set in embedding space. These findings validate that the diffusion-generated augmentations are independent of the downstream task's test set, ensuring the integrity of the evaluation process.

A.3 Computational Complexity of `GeNIe` and `GeNIe-Ada`

Here we provide details on the computational complexity of `GeNIe` across multiple noising ratios r and `GeNIe-Ada` when operating on a search space of $r \in [0.6, 0.8]$. Computational complexity has been reported in terms of the total number of inference/denoising-diffusion steps and the runtime in seconds per generated image. The runtime has been averaged over 10 different image-generations on an NVIDIA Tesla-V100 GPU with 16GB VRAM with 50 steps of denoising using a DPM scheduler with StableDiffusion v1.5. As can be seen in Tab. A1, `GeNIe` is approximately $1/r$ times faster than the base diffusion model (referred to as the `Txt2Img` augmentation baseline). This empirically corroborates with the total number of denoising steps using in `GeNIe` vs. `Txt2Img`. Since, `GeNIe-Ada` scans for the best hard-negative in $r \in [0.6, 0.8]$, it incurs a computational cost of $\approx 2.2\times$ the `Txt2Img`. Note that the runtime for `GeNIe-Ada` reported in Tab. A1 also includes the runtime of performing a batched forward pass through a ResNet-50 feature extraction backbone.

Table A1: Computational Complexity

Augmentation	**Inf. Steps**	**Runtime [sec/img]**
`Txt2Img`	T	4.12
`GeNIe`(r=0.5)	$0.5 \times T$	2.17
`GeNIe`(r=0.6)	$0.6 \times T$	2.59
`GeNIe`(r=0.7)	$0.7 \times T$	2.98
`GeNIe`(r=0.8)	$0.8 \times T$	3.46
`GeNIe-Ada`	$2.1 \times T$	9.22

A.4 Additional Augmentation Comparisons

We compute few-shot classification scores on mini-ImageNet with additional combinations of traditional augmentations. We introduce a Mixed augmentation scheme where we use a combination of Weak and Strong augmentations together. We also experiment the scenario where CutMix and MixUp are used alongside the Mixed augmentation strategy as indicated by Mixed+CutMix and Mixed+MixUp. Finally, we experiment with a combination of `GeNIe` along with MixUp, similar to (Graikos et al., 2023b). As can be seen in Tab. A2, we notice marginal improvements of upto 0.6% by using the Mixed augmentations either with or without the CutMix, MixUp counterparts. We also notice a drop in performance of upto 0.9% when MixUp is used along with `GeNIe`. This follows the general trend of drop in performance when using CutMix or MixUp, as reported in Tab. 1.

A.5 Effect of Backbone for Noise Ratio Selector in `GeNIe-Ada`

To analyze the effect of the backbone feature extractor f_θ on selecting the optimal hard-negative using `GeNIe-Ada`, we use a pre-trained DeiT-B (Touvron et al., 2021a) instead of the UniSiam pretrained ResNet

Table A2: ***mini*-ImageNet:** We use our augmentations on (5-way, 1-shot) and (5-way, 5-shot) few-shot settings of mini-Imagenet dataset with 2 different backbones (ResNet-18 and 50). We compare with additional combinations of traditional augmentations, with and without `GeNIe`. The number of generated images per class is 4 for 1-shot and 20 for 5-shot settings.

ResNet-18				
Augmentation	**Method**	**Pre-training**	**1-shot**	**5-shot**
Weak	UniSiam 2022	unsup.	63.1±0.8	81.4±0.5
Strong	UniSiam 2022	unsup.	62.8±0.8	81.2±0.6
Mixed	UniSiam 2022	unsup.	63.2±0.5	81.9±0.4
CutMix 2019a	UniSiam 2022	unsup.	62.7±0.8	80.6±0.6
MixUp 2018	UniSiam 2022	unsup.	62.1±0.8	80.7±0.6
Mixed+MixUp 2018	UniSiam 2022	unsup.	65.7±0.9	82.1±0.2
Mixed+CutMix 2018	UniSiam 2022	unsup.	64.9±0.8	81.6±0.5
DAFusion 2024	UniSiam 2022	unsup.	64.3±1.8	82.0±1.4
`GeNIe`+MixUp	UniSiam 2022	unsup.	74.8±0.5	84.5±0.3
`GeNIe` (Ours)	UniSiam 2022	unsup.	**75.5±0.6**	**85.4±0.4**
`GeNIe-Ada` (Ours)	UniSiam 2022	unsup.	**76.8±0.6**	**85.9±0.4**

ResNet-50				
Augmentation	**Method**	**Pre-training**	**1-shot**	**5-shot**
Weak	UniSiam 2022	unsup.	64.6±0.8	83.4±0.5
Strong	UniSiam 2022	unsup.	64.8±0.8	83.2±0.5
Mixed	UniSiam 2022	unsup.	64.5±0.5	83.8±0.5
CutMix 2019a	UniSiam 2022	unsup.	64.3±0.8	83.2±0.5
MixUp 2018	UniSiam 2022	unsup.	63.8±0.8	84.6±0.5
Mixed+MixUp 2018	UniSiam 2022	unsup.	64.9±0.7	84.5±0.7
Mixed+CutMix 2018	UniSiam 2022	unsup.	63.5±0.5	83.0±0.8
DAFusion 2024	UniSiam 2022	unsup.	65.7±1.8	83.9±1.2
`GeNIe`+MixUp	UniSiam 2022	unsup.	76.4±0.5	85.9±0.7
`GeNIe` (Ours)	UniSiam 2022	unsup.	**77.3±0.6**	**87.2±0.4**
`GeNIe-Ada` (Ours)	UniSiam 2022	unsup.	**78.6±0.6**	**87.9±0.4**

backbone. However, we still utilize the same ResNet backbone for few-shot classification. As shown in Tab. A3, we notice a marginal improvement of upto 0.7% when using `GeNIe-Ada`+DeiT-B as compared to `GeNIe-Ada` which uses the UniSiam pre-trained ResNet backbone. This suggests that there is still potential to develop more effective strategies for selecting noise ratios to further enhance `GeNIe`. However, in this paper, we limit our exploration to `GeNIe-Ada` and leave these improvements for future work.

Table A3: **Effect of Backbone for Noise Ratio Selector in `GeNIe-Ada`:** We evaluate the impact of the noise ratio selector used in `GeNIe-Ada` ($f_\theta(.)$). Note that in all experiments presented in this paper, we use the same backbone for $f_\theta(.)$ that is subsequently fine-tuned for few-shot classification tasks. However, to analyze the effect of $f_\theta(.)$ on sampled augmentations, we replace it with a more powerful backbone, specifically DeiT-B pretrained on ImageNet-1K. It is important to note that this is not a practical assumption; if DeiT-B were available for noise selection, it could also be used as the classifier in few-shot experiments, outperforming the weaker backbones employed in our study. Nevertheless, this experiment demonstrates that using a stronger backbone can result in more accurate selection of augmentations in `GeNIe`, thereby enhancing the final accuracy. To clarify, DeiT-B is utilized solely as $f_\theta(.)$ for sampling augmentations and not as the classifier. Therefore, the observed improvement is attributed exclusively to better augmentation sampling.

ResNet-18				
Augmentation	**Noise Ratio Selector Backbone $f_\theta(.)$**	**Method [Classifier Backbone]**	**1-shot**	**5-shot**
`GeNIe` (Ours)	-	UniSiam[ResNet18]	**75.5±0.6**	**85.4±0.4**
`GeNIe-Ada`	UniSiam[ResNet18]	UniSiam[ResNet18]	**76.8±0.6**	**85.9±0.4**
`GeNIe-Ada`	IN-1K[DeiT-B]	UniSiam[ResNet18]	**77.5±0.5**	**86.3±0.2**

ResNet-50				
Augmentation	**Noise Selector Backbone $f_\theta(.)$**	**Method [Classifier Backbone]**	**1-shot**	**5-shot**
`GeNIe`	-	UniSiam[ResNet50]	**77.3±0.6**	**87.2±0.4**
`GeNIe-Ada`	UniSiam[ResNet50]	UniSiam[ResNet50]	**78.6±0.6**	**87.9±0.4**
`GeNIe-Ada`	IN-1K[DeiT-B]	UniSiam[ResNet50]	**79.2±0.4**	**88.3±0.5**

A.6 Impact of GeNIe with Fine-Tuning:

For all our experiments regarding `GeNIe` and `GeNIe-Ada`, we assume that the base diffusion model is aware/has been trained on some samples of the target class. This facilitates the addition of the target class (input as text-prompt) into the generated augmentation, while retaining the low-level features of the source image through partial noising. However, there can be a scenario where the base diffusion model does not understand the contradictory text prompt and thus fails to incorporate it into the generated image. As a solution, we can use textual inversion (Gal et al., 2022b) to fine-tune the diffusion model on few images belonging the unknown target class to learn the corresponding embeddings for the target categories. This fine-tuning allows us to learn embeddings specific to the target class, enabling the generation of the desired hard-negative examples. To empirically demonstrate the robustness of `GeNIe` on these scenarios, we present few-shot classification results on mini-Imagenet using `GeNIe` hard-negative augmentations in Tab. A4, generated by textual-inversion fine-tuning the diffusion model on images of the target class. Note that once the diffusion model is fine-tuned, the procedure to generate hard-negatives using partial noising and a contradictory text-prompt remains the same. As can be seen in Tab. A4, `GeNIe`+TxtInv performs significantly better than DAFusion baseline. It is important to note that, in this case, we do not utilize any information about the target category labels. DAFusion also employs textual-inversion-based fine-tuning; however, it does so without generating hard-negative samples. This indicates that GeNIe is effective even in scenario where the diffusion model is unaware of the target-class.

Table A4: ***mini*-ImageNet:** We use our augmentations on (5-way, 1-shot) and (5-way, 5-shot) few-shot settings of mini-Imagenet dataset with 2 different backbones (ResNet-18 and 50), by using Textual-Inversion (Gal et al., 2022b) on the target-classes. The number of generated images per class is 4 for 1-shot and 20 for 5-shot settings.

ResNet-18				
Augmentation	**Method**	**Pre-training**	**1-shot**	**5-shot**
DAFusion 2024	UniSiam 2022	unsup.	64.3±1.8	82.0±1.4
`GeNIe`+TxtInv	UniSiam 2022	unsup.	**73.9±0.8**	**84.6±0.9**

ResNet-50				
Augmentation	**Method**	**Pre-training**	**1-shot**	**5-shot**
DAFusion 2024	UniSiam 2022	unsup.	65.7±1.8	83.9±1.2
`GeNIe`+TxtInv	UniSiam 2022	unsup.	**76.2±1.2**	**86.2±0.9**

A.7 Details of Fine-grained Few-shot Classification

Here we provide details of Fine-grained Few-shot Classification experiments.

Datasets: We assess our method on several datasets: Food101 (Bossard et al., 2014) with 101 classes of foods, CUB200 (Wah et al., 2011) with 200 bird species classes, Cars196 (Krause et al., 2013) with 196 car model classes, and FGVC-Aircraft (Maji et al., 2013) with 41 aircraft manufacturer classes. We provide detailed information around fine-grained datasets in Table A5. The reported metric is the average Top-1 accuracy over 100 episodes. Each episode involves sampling 20 classes and 1-shot from the training set, with the final model evaluated on the respective test set.

Implementation Details: We enhance the basic prompt by incorporating the superclass name for the fine-grained dataset: "A photo of a <`target class`>, a type of <`superclass`>". For instance, in the *food* dataset and the *burger* class, our prompt reads: "A photo of a *burger*, a type of *food*." No additional augmentation is used for generative methods in this context. We generate 19 samples for both cases of our method and also the baseline with weak augmentation.

Table A5: Train and test split details of the fine-grained datasets. We use the provided train set for few-shot task generation, and the provided test sets for our evaluation. Aircraft dataset uses the manufacturer hierarchy.

Dataset	Classes	Train samples	Test samples
CUB200 (Wah et al., 2011)	200	5994	5794
Food101 (Bossard et al., 2014)	101	75750	25250
Cars (Krause et al., 2013)	196	8144	8041
Aircraft (Maji et al., 2013)	41	6,667	3333

A.8 Few-shot Classification with ResNet-34 on *tiered*Imagenet

Table A6: ***tiered*-ImageNet:** Accuracies (% ± std) for 5-way, 1-shot and 5-way, 5-shot classification settings on the test-set. We compare against various SOTA supervised and unsupervised few-shot classification baselines as well as other augmentation methods, with UniSiam (Lu et al., 2022) pre-trained ResNet-34 backbone.

ResNet-34				
Augmentation	**Method**	**Pre-training**	**1-shot**	**5-shot**
Weak	MAML + dist (Finn et al., 2017)	sup.	51.7±1.8	70.3±1.7
Weak	ProtoNet (Snell et al., 2017)	sup.	52.0±1.2	72.1±1.5
Weak	UniSiam + dist (Lu et al., 2022)	unsup.	68.7±0.4	85.7±0.3
Weak	UniSiam (Lu et al., 2022)	unsup.	65.0±0.7	82.5±0.5
Strong	UniSiam (Lu et al., 2022)	unsup.	64.8±0.7	82.4±0.5
CutMix (Yun et al., 2019a)	UniSiam (Lu et al., 2022)	unsup.	63.8±0.7	80.3±0.6
MixUp (Zhang et al., 2018)	UniSiam (Lu et al., 2022)	unsup.	64.1±0.7	80.0±0.6
`Img2Img`^{L}(Luzi et al., 2022)	UniSiam (Lu et al., 2022)	unsup.	66.1±0.7	83.1±0.5
`Img2Img`^{H}(Luzi et al., 2022)	UniSiam (Lu et al., 2022)	unsup.	70.4±0.7	84.7±0.5
`Txt2Img`(He et al., 2022b)	UniSiam (Lu et al., 2022)	unsup.	75.0±0.6	85.4±0.4
DAFusion (Trabucco et al., 2024)	UniSiam (Lu et al., 2022)	unsup.	64.1±2.1	82.8±1.4
`GeNIe` (Ours)	UniSiam (Lu et al., 2022)	unsup.	**75.7±0.6**	**86.0±0.4**
`GeNIe-Ada` (Ours)	UniSiam (Lu et al., 2022)	unsup.	**76.9±0.6**	**86.3±0.2**

We follow the same evaluation protocol here as mentioned in section 4.1. As summarized in Table A6, `GeNIe` and `GeNIe-Ada` outperform all other data augmentation techniques.

Table A7: Few-shot classification comparison of GeNIe-Ada with `Txt2Img` on miniImagenet.

Method	ResNet-18		ResNet-34		ResNet-50	
	1-shot	5-shot	1-shot	5-shot	1-shot	5-shot
`Txt2Img`	76.9±1.0	86.5±0.9	77.1±0.8	86.7±1.0	77.2±1.3	86.8±0.9
`GeNIe-Ada`	77.7±0.8	87.4±1.0	78.3±0.9	87.8±0.9	79.1±1.1	88.4±1.2

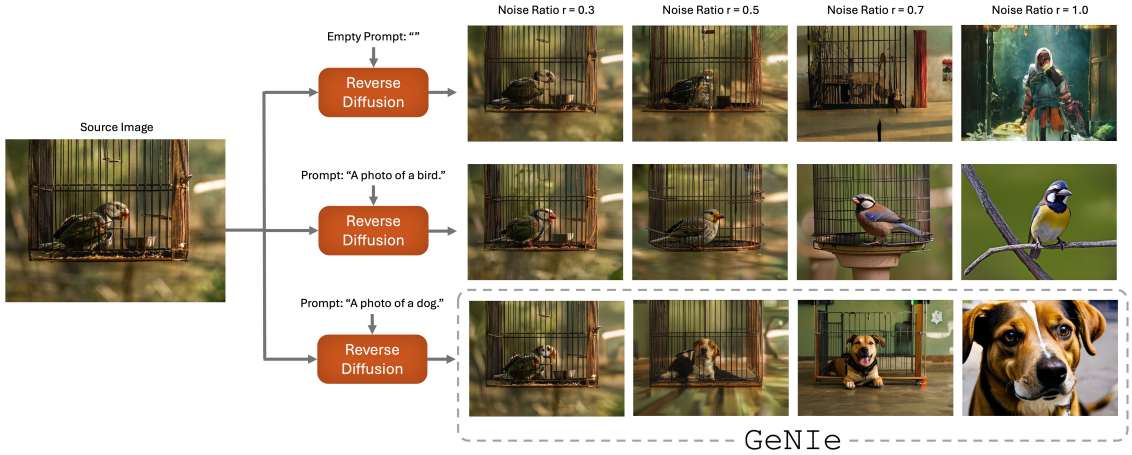

Figure A4: **Key components of `GeNIe`:** (i) careful choice of r and (ii) contradictory prompt are two key idea behind `GeNIe`

Figure A5: Analyzing the semantic trajectory of `GeNIe` augmentations across 10 different images of class Mushroom (source image) to class Volcano (target class).

A.9 Additional details of Long-Tail experiments

We present a comprehensive version of Table 4 to benchmark the performance with different backbone architectures (e.g., ResNet50) and to compare against previous long-tail baselines; this is detailed in Table A8.

Implementation Details of LViT: We download the pre-trained ViT-B of LViT (Xu et al., 2023) and finetune it with Bal-BCE loss proposed therein on the augmented dataset. Training takes 2 hours on four NVIDIA RTX 3090 GPUs. We use the same hyperparameters as in (Xu et al., 2023) for finetuning: 100 epochs, $lr = 0.008$, batch size of 1024, CutMix and MixUp for the data augmentation.

Implementation Details of VL-LTR: We use the official code of VL-LTR (Tian et al., 2022) for our experiments. We use a pre-trained CLIP ResNet-50 backbone. We followed the hyperparameters reported in VL-LTR (Tian et al., 2022). We augment only "Few" category and train the backbone with the VL-LTR (Tian et al., 2022) method. Training takes 4 hours on 8 NVIDIA RTX 3090 GPUs.

A.10 Extra Computation of GeNIe-Ada

Given that GeNIe-Ada searches for the best hard-negative between multiple noise-ratios r's, it naturally requires a higher compute budget than `txt2Img` that only uses $r = 1$. For this experiment, we use GeNIe-Ada with $r \in \{0.6, 0.7, 0.8\}$ to compare with `Txt2Img`. Based on this, we only have 3 paths, with steps of 0.1), and for each of which we go through partial reverse diffusion process. E.g. for $r = 0.6$ we do 30 steps instead of standard 50 steps of Stable Diffusion. This practically breaks down the total run-time of `GeNIe-Ada` to approximately 2 times that of the standard reverse diffusion (GeNIe-Ada: total $r = 0.6 + 0.7 + 0.8 = 2.1$ vs `Txt2Img` total $r = 1$). Thus, to be fair, we generate twice as many `Txt2Img` augmentations as compared to GeNIe-Ada to keep a constant compute budget across the methods, following your suggestion. The results are shown in Table A7. As can be seen, even in this new setting, GeNIe-Ada offers a performance improvement of 0.8% to 1.9% across different backbones.

Table A8: **Long-Tailed ImageNet-LT:** We compare different augmentation methods on ImageNet-LT and report Top-1 accuracy for "Few", "Medium", and "Many" sets. † indicates results with ResNeXt50. $*$: indicates training with 384 resolution so is not directly comparable with other methods with 224 resolution. On the "Few" set and LiVT method, our augmentations improve the accuracy by 11.7 points compared to LiVT original augmentation and 4.4 points compared to `Txt2Img`.

ResNet-50				
Method	Many	Med.	Few	Overall Acc
CE (Cui et al., 2019)	64.0	33.8	5.8	41.6
LDAM (Cao et al., 2019)	60.4	46.9	30.7	49.8
c-RT (Kang et al., 2020)	61.8	46.2	27.3	49.6
τ-Norm (Kang et al., 2020)	59.1	46.9	30.7	49.4
Causal (Tang et al., 2020)	62.7	48.8	31.6	51.8
Logit Adj. (Menon et al., 2021)	61.1	47.5	27.6	50.1
RIDE(4E)† (Wang et al., 2021)	68.3	53.5	35.9	56.8
MiSLAS (Zhong et al., 2021)	62.9	50.7	34.3	52.7
DisAlign (Zhang et al., 2021a)	61.3	52.2	31.4	52.9
ACE† (Cai et al., 2021)	71.7	54.6	23.5	56.6
PaCo† (Cui et al., 2021a)	68.0	56.4	37.2	58.2
TADE† (Zhang et al., 2021b)	66.5	**57.0**	43.5	58.8
TSC (Li et al., 2022f)	63.5	49.7	30.4	52.4
GCL (Li et al., 2022e)	63.0	52.7	37.1	54.5
TLC (Li et al., 2022a)	68.9	55.7	40.8	55.1
BCL† (Zhu et al., 2022)	67.6	54.6	36.6	57.2
NCL (Li et al., 2022c)	67.3	55.4	39.0	57.7
SAFA (Hong et al., 2022)	63.8	49.9	33.4	53.1
DOC (Wang et al., 2022)	65.1	52.8	34.2	55.0
DLSA (Xu et al., 2022)	67.8	54.5	38.8	57.5
ResLT (Cui et al., 2022)	63.3	53.3	40.3	55.1
PaCo (Cui et al., 2021b)	68.2	58.7	41.0	60.0
LWS (Kang et al., 2019)	62.2	48.6	31.8	51.5
Zero-shot CLIP (Radford et al., 2021)	60.8	59.3	58.6	59.8
DRO-LT (Samuel & Chechik, 2021)	64.0	49.8	33.1	53.5
VL-LTR (Tian et al., 2022)	77.8	67.0	50.8	70.1
Cap2Aug (Roy et al., 2023)	78.5	**67.7**	51.9	70.9
`GeNIe-Ada`	**79.2**	64.6	**59.5**	**71.5**
ViT-B				
LiVT* (Xu et al., 2023)	76.4	59.7	42.7	63.8
ViT (Dosovitskiy et al., 2021)	50.5	23.5	6.9	31.6
MAE (He et al., 2022a)	74.7	48.2	19.4	54.5
DeiT (Touvron et al., 2022)	70.4	40.9	12.8	48.4
LiVT (Xu et al., 2023)	73.6	56.4	41.0	60.9
LiVT + `Img2Img`^{L}	74.3	56.4	34.3	60.5
LiVT + `Img2Img`^{H}	73.8	56.4	45.3	61.6
LiVT + `Txt2Img`	**74.9**	55.6	48.3	62.2
LiVT + `GeNIe` (r=0.8)	74.5	56.7	50.9	62.8
LiVT + `GeNIe-Ada`	74.0	**56.9**	**52.7**	**63.1**

A.11 Further analysis of semantic shifts using GeNIe

In Fig. 5, we empirically demonstrate that by increasing the noise ratio from 0 to 1, the semantic category of the source image transitions gradually from the source class to the text-prompt's target class. To establish this further, we now choose 10 samples of a source class of Mushroom and generate GeNIe augmentations with the target class of a Volcano. The generated images corresponding to each $r \in [0, 1]$ are passed through a DINOv2 encoder and their embeddings are projected onto their 2 principle eigen vectors using PCA. The trajectories extracted from each of these 10 source images is depicted collectively and individually in Fig. A5. It can be noticed that each of the trajectories demonstrate a gradual transition of semantic category from the source to the target class, with a sparse distribution of points usually observed within $[0.4, 0.6]$. This is also observed in the plot on the bottom-right side of the figure where all trajectories are collectively plotted. Here, however, there is no clear range of r where a sparse distribution of points can be observed, thus indicating that each source image has its own optimal r value. This can be attributed to the inter-sample variances of images belonging to the same class. Since GeNIe-Ada operates on each individual source image and target class text-prompt, it facilitates the selection of the best hard-negative per sample.

A.12 How does GeNIe control which features are retained or changed?

We instruct the diffusion model to generate an image by combining the latent noise of the source image with the textual prompt of the target category. This combination is controlled by the amount of added noise and the number of reverse diffusion iterations. This approach aims to produce an image that aligns closely with the semantics of the target category while preserving the background and features from the source image that are unrelated to the target.

To demonstrate this, in Figure A4, We are progessivley moving towards the two key components of GeNIe: (i) careful choice of r and (ii) contradictory prompt. The input image is a bird in a cage. The top row shows a Stable Diffusion model, unprompted. As can be seen, such a model can generate anything (irrespective of the input image) with a large r. Now prompting the same model with "a photo of a bird" allows the model to preserve low-level and contextual features of the input image (up to $r = 0.7$ and 0.8), until for a large $r \geq 0.9$ it returns a bird but the context has nothing to do with the source input. This illustrates how a careful choice of r can help preserve such low-level features, and is a key idea behind GeNIe. However, we also need a semantic switch to a different target class as shown in the last row where a hardly seen image of a dog in a cage is generated by a combination of a careful choice of r and the contradictory prompt - leading to the full mechanics of GeNIe. This sample now serves as hard negative for the source image (bird class).

A.13 Analyzing Noise Effects in Bi-Directional Transformations with GeNIe

To further explore the effect of noise ratio r in GeNIe, we conducted an experiment where GeNIe was applied twice to transform between a source image and a target category. For this experiment, images from the "mushroom" category were used as the source, and "volcano" served as the target category. In the first step, we applied GeNIe using a mushroom image as the source and a volcano prompt as the target. In the second step, we reversed the process: the GeNIe-generated volcano image from the first step was used as the source, with the target prompt set to mushroom. Importantly, using a smaller noise ratio, r during the generation of the volcano image helps preserve more low-level visual features from the original mushroom source image. Consequently, when the roles of source and target are flipped in the second step, the final image retains a stronger resemblance to the original mushroom source image for lower noise ratios. This phenomenon is visualized in Fig. A6. As shown, a lower noise ratio during the first step results in the preservation of more visual features, leading to a final image that more closely resembles the original mushroom source.

A.14 More Visualizations

Additional qualitative results resembling the style presented in Fig. 4 are presented in Fig. A8, and more visuals akin to Fig. 2 can be found in Fig. A9. Moreover, we also present more visualization similar to the style in Fig. 5 in Fig. A7.

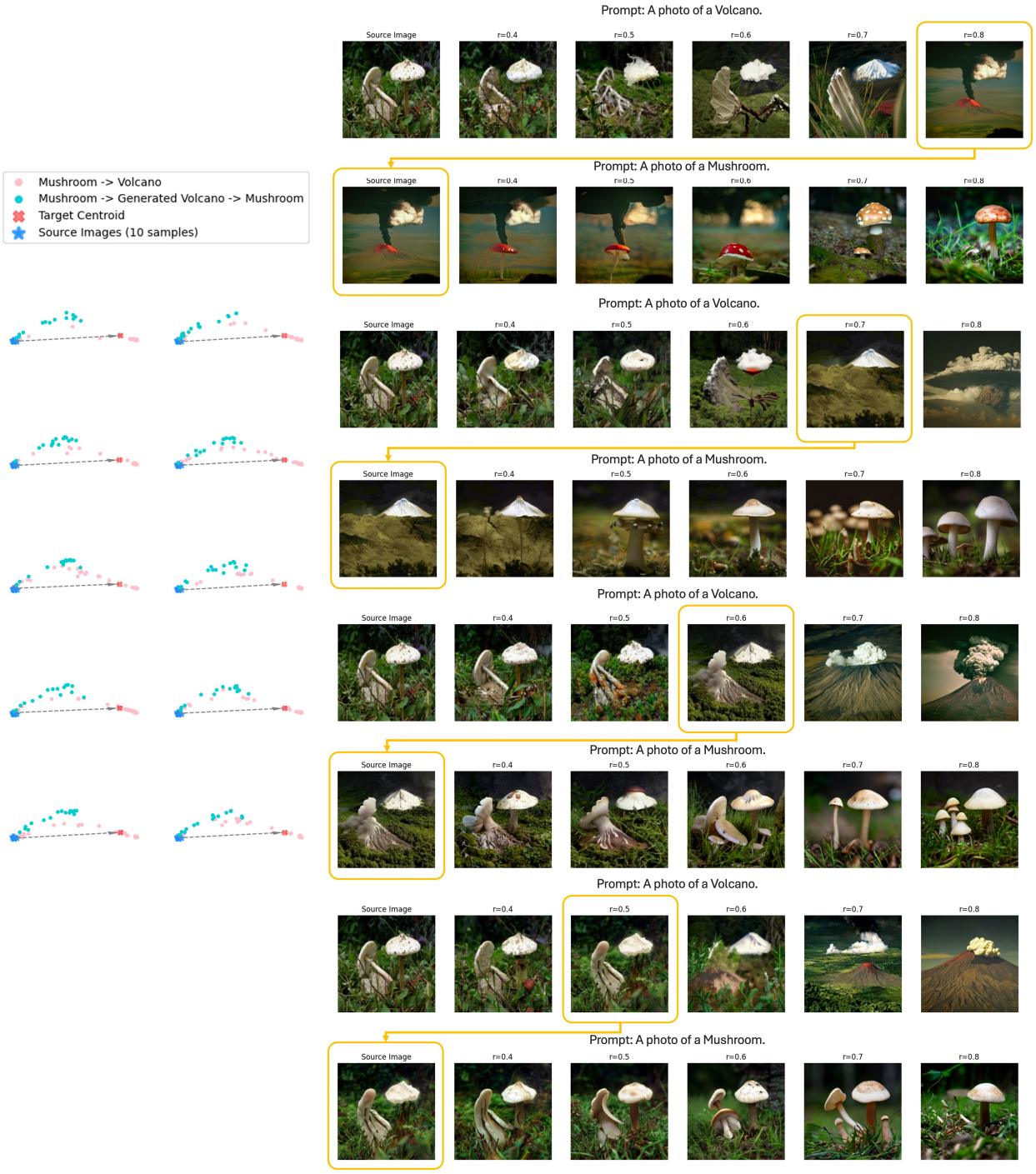

Figure A6: **Trajectory of `GeNIe` augmentations:** To further analyze the effect of noise ratio r in `GeNIe`, we conducted an experiment using a set of augmentations generated from 10 different source images in the "mushroom" category, with a target label of "Volcano," across varying noise ratios. Similar to Fig. 5, all generated augmentations were processed through the DinoV2 ViT-G model, which serves as our oracle, to extract their embeddings. For visualization, we applied PCA to these embeddings. Next, we selected one augmentation with a specific noise ratio, (r), and used it as the source image in for the "volcano" category in `GeNIe`, with the target prompt set to "mushroom." As observed, using a lower noise ratio samples as the source for "volcano" preserves more low-level visual features from the original mushroom source image. Consequently, after a second round of applying `GeNIe`, the resulting augmentations (even rows) tend to more closely resemble the original source image (first image in the corresponding odd rows above). The left plot presents the embeddings of all 10 samples, while the right plot provides a detailed visualization of one sample, showcasing the impact of varying noise ratios used in the second step of applying `GeNIe`.

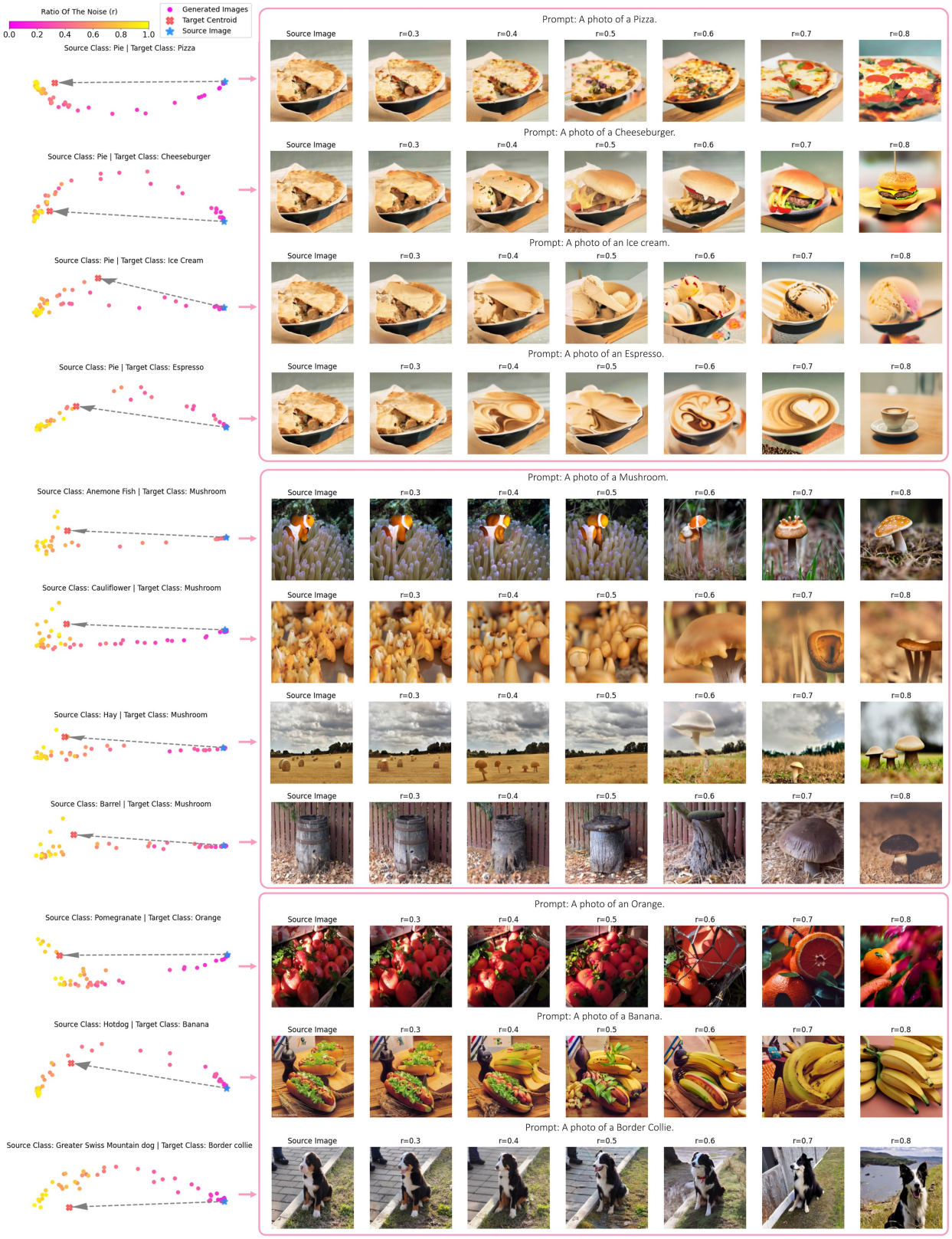

Figure A7: **Effect of noise in `GeNIe`:** Similar to Fig. 5, we pass all the generated augmentations through the DinoV2 ViT-G model, which acts as our oracle model, to obtain their associated embeddings. Subsequently, we employ PCA for visualization purposes. The visualization reveals that the magnitude of semantic transformations is contingent upon both the source image and the specified target category.

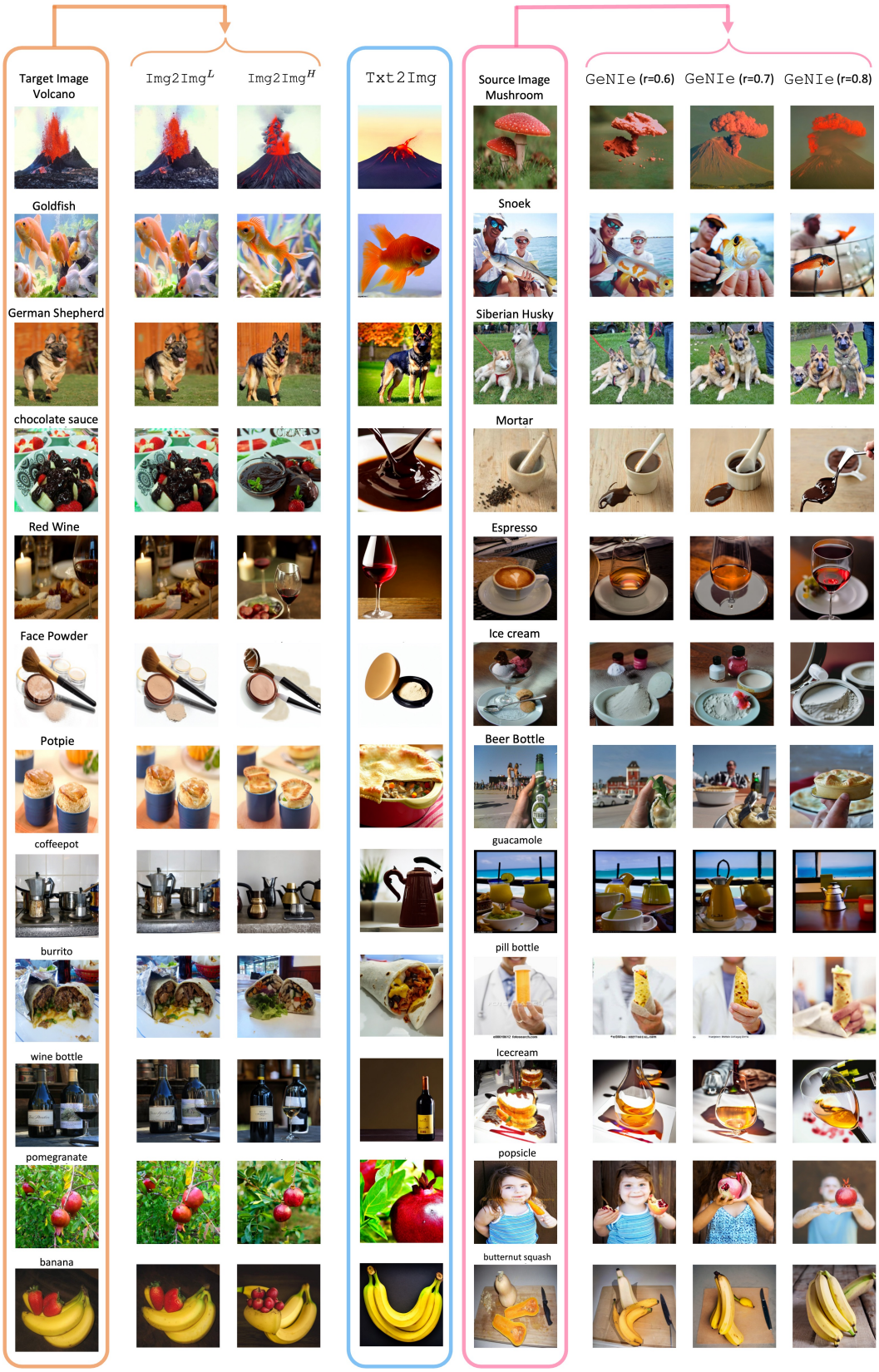

Figure A8: **Visualization of Generative Samples:** More visualization akin to Fig. 4. We compare **GeNIe** with two baselines: **Img2Img^L augmentation** uses both image and text prompt from the same category, resulting in less challenging examples. **Txt2Img augmentation** generates images based solely on a text prompt, potentially deviating from the task's visual domain. **GeNIe augmentation** incorporates the target category name in the text prompt along with the source image, producing desired images with an optimal amount of noise, and balancing the impact of the source image and text prompt.

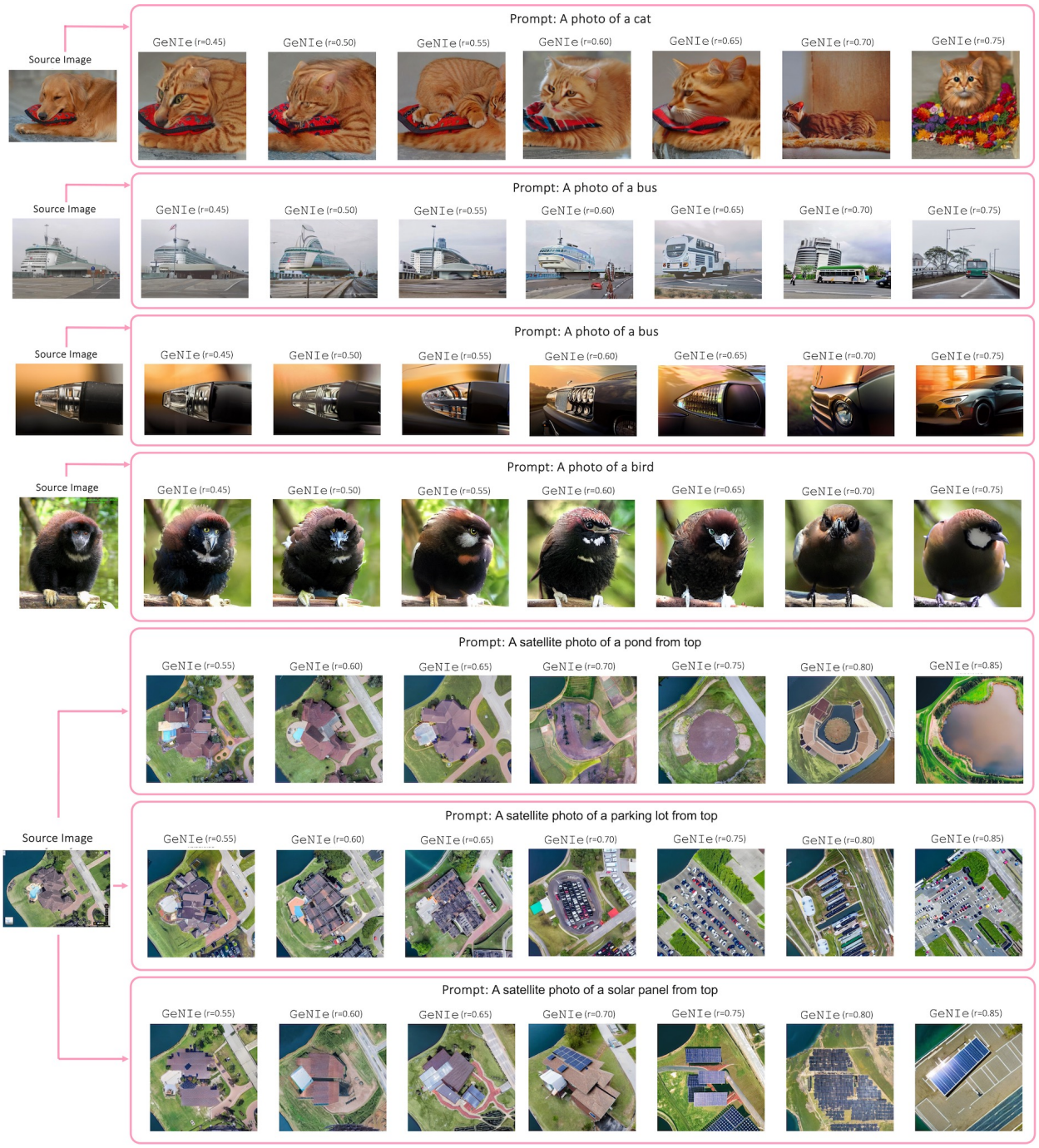

Figure A9: **Effect of noise in `GeNIe`:** Akin to Fig. 2, we use `GeNIe` to create augmentations with varying noise levels. As is illustrated in the examples above, a reduced amount of noise leads to images closely mirroring the semantics of the source images, causing a misalignment with the intended target label.